



**Ana Sofia Domingues Santos Saraiva**

Licenciada em Biologia Celular e Molecular

**Polylactic acid 3D scaffolds as platforms for  
local-delivery and hyperthermia applications  
in bone tumours**

Dissertação para obtenção do Grau de Mestre em  
Genética Molecular e Biomedicina

Orientador: Ana Bettencourt, Professora Doutora, Faculdade de  
Farmácia, Universidade de Lisboa

Co-orientador: Lídia Gonçalves, Professora Doutora, Faculdade  
de Farmácia, Universidade de Lisboa

Júri:

Presidente: Doutora Maria Alexandra Núncio de Carvalho Ramos Fernandes

Arguente: Doutor Pedro Miguel Ribeiro Viana Baptista

Vogal: Doutora Ana Francisca de Campos Simão Bettencourt





**Ana Sofia Domingues Santos Saraiva**

Licenciada em Biologia Celular e Molecular

**Polylactic acid 3D scaffolds as platforms for  
local-delivery and hyperthermia applications  
in bone tumours**

Dissertação para obtenção do Grau de Mestre em  
Genética Molecular e Biomedicina

Orientador: Ana Bettencourt, Professora Doutora, Faculdade de  
Farmácia, Universidade de Lisboa

Co-orientador: Lídia Gonçalves, Professora Doutora, Faculdade  
de Farmácia, Universidade de Lisboa

Júri:

Presidente: Doutora Maria Alexandra Núncio de Carvalho Ramos Fernandes

Arguente: Doutor Pedro Miguel Ribeiro Viana Baptista

Vogal: Doutora Ana Francisca de Campos Simão Bettencourt



**Polylactic acid 3D scaffolds as platforms for local-delivery and hyperthermia applications in bone tumours**

Copyright © Ana Sofia Domingues Santos Saraiva, Faculdade de Ciências e Tecnologia, Universidade Nova de Lisboa.

A Faculdade de Ciências e Tecnologia e a Universidade Nova de Lisboa têm o direito, perpétuo e sem limites geográficos, de arquivar e publicar esta dissertação através de exemplares impressos reproduzidos em papel ou de forma digital, ou por qualquer outro meio conhecido ou que venha a ser inventado, e de a divulgar através de repositórios científicos e de admitir a sua cópia e distribuição com objetivos educacionais ou de investigação, não comerciais, desde que seja dado crédito ao autor e editor.



# Acknowledgments

---

The master thesis presented here would not been possible to accomplish without the support, assistance, encouragement and enter help of all those who have contributed to it, to which I want to express my deepest thanks and respect.

First, I would like to thank to my main supervisor, Dra. Ana Bettencourt, and to my co-supervisor, Dra. Lúcia Gonçalves, for the opportunity to participate in this project, for the advices and guidance along the work, as well as for the understanding given in this year personally difficult. For always been available, for all the teaching and knowledge that was kindly passed to me and that will be very important in the future, for the opportunity to work autonomously permitting to learn how to overcome the problems that arise, but always helping when needed. Throughout this year, it was a privilege to work and spend relaxed moments in their company, knowing it will be two persons I will fondly take for life.

I would also like to thank to Dra. Isabel Ribeiro for welcoming me into her microbiology lab and for the guidance given, and to Dra. Catarina Santos e Dra. Marta Alves for the sympathy, help and support.

Thanks to all members from NanoBB and CBT research groups, as well as to all members of building D of Faculdade de Farmácia for accepting me, for the hospitality and for the companionship. A special thanks to Victor Martin for the knowledge passed and for the good mood that spreads to all.

Thanks to both institutions, Faculdade de Farmácia da Universidade de Lisboa and Instituto Superior Técnico da Universidade de Lisboa, for the opportunity to perform the present work and for the technical support given along the work.

A big thank you to my friends and everyday companions in the lab, Inês Anjos e Sandra Cordeiro, for the help and for the good and happy moments shared.

For always being there, thanks to the friends that university gave me, Cláudia Fernandes and specially to Inês Pombo for the encouragement, motivation and patience.

Thanks to my mother and father for the opportunities they gave me and for the unconditional support and pride. Also, thank you to my closest family: grandparents, uncles and cousins.

Thank you to Gustavo Dinis for being always present and supportive, for helping in the toughest times and for the unconditional love.

At last, thanks to my oldest friends, Catarina Pires, Filipa Pedroso, João Cortes and Guilherme Rodrigues that accompanied me not only this year, but my whole life, for the happy distractions. A special thanks to Catarina Pires for the help with english questions.

## Funding:

This work was financial supported by UID/DTP/04138/2019 and UID/QUI/00100/2019 from Fundação para a Ciência e Tecnologia (FCT).



# Abstract

---

The bone is one of the most frequent target sites of metastases. Presently, treatment management has a variety of limitations that need to be replaced by more effective strategies. In this context, three-dimensional (3D) printed scaffolds can be an adjuvant local therapy for bone metastases as well as accomplish several biological and mechanical requirements for bone regeneration with the additional possibility of design the architecture of the scaffold according to the patient's needs. In this study, 3D-printed PLA scaffolds were multifunctionalized with: i) collagen (Col) and hydroxyapatite nanoparticles (nHA) aiming the promotion of bone regeneration, ii) superparamagnetic iron oxide nanoparticles (SPIONs) for magnetic hyperthermia purposes against bone tumour cells and iii) minocycline (MH) to prevent bone infection. The physicochemical properties, *in vitro* swelling ability, drug (MH) release, bioactivity, magnetic heating properties, antimicrobial properties and cell response of functionalized PLA scaffolds were investigated. Results showed that scaffolds were obtained with uniform square macroporous and a stable functionalization. Also, a properly low swelling ability for bone regeneration and bioactive properties specially with the presence of nHA was attained. MH functionalization resulted into an efficient antibacterial activity against *Staphylococcus aureus*, a pathogen often associated with bone-related infections, that was coupled with an adequate drug release profile leading to an effective prevention of bone infection. PLA scaffolds revealed to be no cytotoxic for cells (MG-63 osteoblasts) and had a higher osteogenic potential when loaded with nHA. SPIONs demonstrated magnetic heating ability, however at the tested concentrations did not reached hyperthermia temperatures (40-45°C). Therefore, multifunctionalized 3D printed PLA scaffolds showed to be a promising strategy for bone regeneration associated with infection prevention and bone cancer treatment with the need to improve on the magnet heating ability of SPIONs to advance bone tumours management.

**Keywords:** Bone cancer, Bone regeneration, Polylactic acid (PLA), Iron oxide nanoparticles, Hydroxyapatite nanoparticles, Magnetic hyperthermia



# Resumo

---

O cancro ósseo secundário, resultante de metástases de outros cancros existentes, é uma patologia bastante frequente, e para o qual o tratamento atualmente disponível apresenta diversas limitações, motivando o desenvolvimento de alternativas mais eficazes. Neste contexto, *scaffolds* obtidos por impressão tridimensional (3D) podem ser explorados como terapia adjuvante localizada em metástases ósseas, assim como, apresentar propriedades biológicas e mecânicas adequadas à regeneração óssea com a possibilidade adicional de delinear a arquitetura do *scaffold* de acordo com as necessidades do paciente. No presente estudo, *scaffolds* de ácido polilático (PLA) impressas em 3D foram funcionalizados com: i) colagénio (Col) e nanopartículas de hidroxiapatite (nHA) com o objetivo de promover a regeneração óssea, ii) nanopartículas de óxido de ferro superparamagnéticas (SPIONs) visando o tratamento de células cancerígenas através de hipertermia magnética e iii) minociclina (MH) para prevenir o desenvolvimento de infeções ósseas. As propriedades físico-químicas, a capacidade de reter água, a libertação do fármaco (MH), a bioatividade, as propriedades magnéticas de aquecimento, as propriedades antibacterianas e a resposta celular *in vitro* dos *scaffolds* de PLA foram investigadas. Os resultados mostraram que os *scaffolds* foram obtidos com macroporos quadrados e uniformes e com uma funcionalização estável. Observou-se ainda que os *scaffolds* apresentaram uma baixa capacidade de retenção de água, adequada para a regeneração óssea, e propriedades bioativas, especialmente na presença de nHA. A funcionalização com MH resultou numa atividade antibacteriana adequada contra *Staphylococcus aureus*, um microrganismo comumente isolado em infeções ósseas. A atividade antibacteriana associada a um perfil de libertação do antibiótico adequada, sugere uma prevenção eficiente de infeções ósseas. Os *scaffolds* de PLA revelaram não ser citotóxicos para as células testadas (osteoblastos MG-63) e apresentaram um potencial osteogénico superior quando carregados com nHA. As SPIONs demonstraram possuir propriedades de aquecimento magnético, no entanto, nas concentrações testadas não foram capazes de alcançar as temperaturas de hipertermia (40-45°C). Concluindo, *scaffolds* de PLA obtidos por impressão 3D e funcionalizados mostraram ser uma possível estratégia promissora para a regeneração óssea associada à prevenção da infeção e ao tratamento do cancro ósseo, com a necessidade de melhoramentos na capacidade de aquecimento magnético das SPIONs visando um avanço nas modalidades de tratamento das metástases ósseas.

**Palavras-chave:** Cancro ósseo, Regeneração óssea, Ácido polilático (PLA), Nanopartículas de óxido de ferro, Nanopartículas de hidroxiapatite, Hipertermia magnética



# Index

---

Acknowledgments .....	V
Abstract .....	VII
Resumo .....	IX
Index.....	XI
List of Figures .....	XV
List of Tables .....	XVII
List of Abbreviations .....	XIX
<b>1 Objectives .....</b>	<b>1</b>
<b>2 Introduction .....</b>	<b>3</b>
2.1 Bone and bone diseases .....	3
2.2 Bone tumours: current treatment and limitations .....	4
2.3 Scaffolds development for bone regeneration .....	5
2.3.1 Scaffolds requirements.....	5
2.3.2 Suitable biomaterial.....	6
2.3.3 Fabrication method.....	7
2.4 Enhance osteogenic potential of PLA .....	8
2.5 Hyperthermia and Iron oxide nanoparticles (SPIONs) .....	9
2.6 Prevention of bone infection.....	11
2.7 Cellular assays on PLA scaffolds .....	12
2.7.1 Cytocompatibility evaluation.....	13
2.7.2 Evaluation of osteogenic potential.....	13
<b>3 Materials and methods .....</b>	<b>15</b>
3.1 Materials .....	15
3.2 Cell culture.....	15
3.3 SPIONs fundamental characterization .....	16
3.3.1 Zeta potential of SPIONs.....	16
3.3.2 <i>In vitro</i> evaluation of SPIONs oxidative stress .....	16
3.3.3 <i>In vitro</i> evaluation of SPIONs cytotoxicity.....	16
3.3.4 SPIONs cellular uptake study.....	17

3.4	Preparation and functionalization of PLA scaffolds .....	17
3.4.1	Surface treatment .....	17
3.4.2	Functionalization .....	18
3.5	Characterization of PLA scaffolds .....	19
3.5.1	Morphological and chemical characterization .....	19
3.5.2	Swelling behaviour .....	19
3.5.3	<i>In vitro</i> minocycline release study .....	19
3.5.4	<i>In vitro</i> bioactivity study .....	20
3.6	Microbiological studies: evaluation of the antimicrobial activity .....	21
3.6.1	Agar diffusion assay .....	21
3.6.2	Biofilm inhibition assay .....	21
3.7	<i>In vitro</i> cellular studies .....	22
3.7.1	Cytocompatibility and cell proliferation .....	22
3.7.2	Evaluation of oxidative stress .....	22
3.7.3	Evaluation of PLA scaffolds osteogenic potential .....	22
3.8	Magnetic heating properties – Thermal studies .....	23
3.9	Statistical analysis .....	24
<b>4</b>	<b>Results .....</b>	<b>25</b>
4.1	SPIONs fundamental characterization .....	25
4.1.1	Zeta potential of SPIONs .....	25
4.1.2	<i>In vitro</i> evaluation of SPIONs oxidative stress .....	25
4.1.3	<i>In vitro</i> evaluation of SPIONs cytotoxicity .....	26
4.1.4	SPIONs cellular uptake study .....	27
4.2	Characterization of functionalized PLA scaffolds .....	28
4.2.1	Morphological and chemical characterization .....	28
4.2.2	Swelling behaviour .....	30
4.2.3	<i>In vitro</i> minocycline release study .....	31
4.2.4	<i>In vitro</i> bioactivity study .....	32
4.3	Microbiological studies: evaluation of antimicrobial activity .....	34
4.3.1	Agar diffusion and biofilm inhibition assays .....	34
4.4	<i>In vitro</i> cellular studies .....	35

4.4.1	Cytocompatibility and cell proliferation .....	35
4.4.2	Evaluation of oxidative stress .....	36
4.4.3	Evaluation of PLA scaffolds osteogenic potential .....	37
4.5	Magnetic heating properties – Thermal studies .....	38
<b>5</b>	<b>Discussion .....</b>	<b>41</b>
<b>6</b>	<b>Conclusions .....</b>	<b>47</b>
<b>7</b>	<b>References .....</b>	<b>49</b>
	Appendix A .....	55
	Appendix B .....	57
	Appendix C .....	61



# List of Figures

---

<b>Figure 3.1</b> Schematic representation of scaffolds preparation: Surface treatment and functionalization.....	18
<b>Figure 3.2</b> Isolated heating unit for evaluation of heating properties .....	24
<b>Figure 4.1</b> MG-63 cells ROS production when in contact with SPIONs.....	26
<b>Figure 4.2</b> Evaluation of SPIONs cytotoxicity .....	27
<b>Figure 4.3</b> Cellular localization of SPIONs .....	28
<b>Figure 4.4</b> Morphological characterization of functionalized PLA scaffolds .....	29
<b>Figure 4.5</b> Chemical composition of functionalized PLA scaffolds surface .....	30
<b>Figure 4.6</b> Swelling ability of PLA scaffolds from G1, G5 and PLA with AHT .....	31
<b>Figure 4.7</b> <i>In vitro</i> release profile of MH from PLA scaffolds .....	32
<b>Figure 4.8</b> Bioactivity of G5: PLA-Col-nHA-SPIONs-MH in SBF solution .....	33
<b>Figure 4.9</b> Agar diffusion assay against <i>S. aureus</i> .....	34
<b>Figure 4.10</b> Assessment of biofilm formation on PLA scaffolds surface .....	35
<b>Figure 4.11</b> PLA scaffolds <i>in vitro</i> cytocompatibility .....	36
<b>Figure 4.12</b> MG-63 cells ROS production when in contact with PLA scaffolds.....	37
<b>Figure 4.13</b> Osteogenic capacity of PLA scaffolds .....	38
<b>Figure 4.14</b> Magnetic heating properties .....	39
<b>Figure A1</b> Swelling ability of PLA scaffolds .....	55
<b>Figure B1</b> Bioactivity of PLA scaffolds in SBF solution .....	57
<b>Figure B2</b> Bioactivity of PLA scaffolds in RPMI 1640 medium .....	58
<b>Figure B3</b> Bioactivity of G5: PLA-Col-nHA-SPIONs-MH in RPMI 1640 medium .....	59
<b>Figure B4</b> pH changes of SBF solution and RPMI 1640 medium .....	60



# List of Tables

---

<b>Table 2.1</b> Advantages and limitations of biomaterials for bone regeneration applications.....	6
<b>Table 3.1</b> Groups of scaffolds according to the surface functionalization .....	18
<b>Table 3.2</b> Chemical composition of simulated body fluid (SBF) .....	20
<b>Table 4.1</b> Zeta potential (mean $\pm$ SD) of SPIONs measured in different media (n = 3) .....	25



# List of Abbreviations

---

<b>AHT</b>	Alkali hydrolysis treatment
<b>ALP</b>	Alkaline phosphatase
<b>AMF</b>	Alternating magnetic field
<b>BMP</b>	Bone morphogenic proteins
<b>CAD</b>	Computer assisted design
<b>CAM</b>	Computer assisted manufacturing
<b>CaP</b>	Calcium phosphates
<b>Col</b>	Collagen
<b>CT</b>	Computerized tomography
<b>DCP</b>	Dicalcium phosphate
<b>ECM</b>	Extracellular matrix
<b>EDS</b>	X-ray energy dispersive spectrometer
<b>FDA</b>	Food and drug administration
<b>FDM</b>	Fused deposition modelling
<b>HA</b>	Hydroxyapatite
<b>H<sub>2</sub>-DCFDA</b>	2,7' dichlorodihydrofluorescein diacetate
<b>IONPs</b>	Iron oxide nanoparticles
<b>MH</b>	Minocycline hydrochloride
<b>MNPs</b>	Magnetic nanoparticles
<b>MRI</b>	Magnetic resonance imaging
<b>MSCs</b>	Mesenchymal stem cells
<b>MTT</b>	Thiazolyl blue tetrazolium bromide
<b>nHA</b>	Hydroxyapatite nanoparticles
<b>PCL</b>	Polycaprolactone
<b>PEG</b>	Poly(ethylene glycol)
<b>PGA</b>	Poly(glycolic acid)
<b>PI</b>	Propidium iodide
<b>PLA</b>	Poly(lactic acid)
<b>PLGA</b>	Poly(lactic-co-glycolic acid)

<b>ROS</b>	Reactive oxygen species
<b>RT</b>	Room temperature
<b>SBF</b>	Simulated body fluid
<b>SDS</b>	Sodium dodecyl sulphate
<b>SEM</b>	Scanning electron microscopy
<b>SLA</b>	Stereolithography
<b>SLS</b>	Selective laser sintering
<b>SPIONs</b>	Superparamagnetic iron oxide nanoparticles
<b>TC</b>	Tetracycline
<b>TCP</b>	Tricalcium phosphate
<b>3D</b>	Three-dimensional



# 1 Objectives

The main objective of this thesis is the development of a novel three-dimensional (3D)-printed polymeric polylactic acid (PLA) scaffold loaded with different components, namely collagen (Col), hydroxyapatite nanoparticles (nHA), superparamagnetic iron oxide nanoparticles (SPIONs) and minocycline (MH), as a local delivery tool to overcome the main difficulties associated with the current bone cancer treatment.

Specific aims were:

- Brief characterization studies on SPIONs;
- Characterization of the functionalized scaffolds (morphological, chemical, swelling and drug release studies);
- Bioactivity assessment as an indicator of osteogenic capacity;
- Assessment of the scaffold's antimicrobial activity against *Staphylococcus aureus* (pathogen responsible for bone infections);
- Evaluation of the cytocompatibility and osteogenic capacity of the functionalized PLA scaffolds on MG-63 cells;
- Appraisal of the magnetic heating properties of SPIONs and scaffolds.

The present work is organized in six chapters: 1. Objectives (the present one); 2. Introduction; 3. Materials and Methods; 4. Results; 5. Discussion; 6. Conclusion; and it is complemented with appendixes.



# 2.

## 2 Introduction

The introduction of the work will go through a close overview of the bone cancer treatment limitations and through the search for effective alternatives to each problem found, considering all the characteristics necessary for proper bone regeneration. The materials and techniques promising to be used are also reviewed and chosen through literature search.

### 2.1 Bone and bone diseases

Bones are natural nanostructures composed by organic compounds, as collagen, and inorganic ones, as calcium and phosphate, and have a specific and characteristic structure that allows them to possess high strength while being light weight (1,2). Depending on the body location of the bone, its properties and structure can differ, allowing it to be a versatile tissue with more than one function besides giving mechanical support, namely: supply protection of several organs, assists in movement and provides shape and metabolic function, e.g. storing calcium and other ions, which causes bone to play an important role in mineral homeostasis (1,3).

Composed by osteoblasts, osteocytes and osteoclast, as specialized bone cells, bone can remodel itself to adapt to mechanical stress and to repair small injuries. Osteoblasts are the bone effector cells which are mechanical sensitive and responsible for the synthesis of the components that constitute the extracellular matrix (ECM) of bone, being responsible for bone formation (2–4). Osteocytes are the mature differentiation state of osteoblast and they occupy the lacunae of bones, resulting in a widespread distribution along the bones, enabling them to sense mechanical stress. Osteoclasts are, partly, responsible for bone resorption that is involved in bone remodelling as a response to growth or to a changing in the mechanical stress (2).

Bone has a remarkable healing capacity, but its regenerative characteristic becomes compromised the greater the damage, requiring a substrate to give support and to guide bone regeneration (5,6). Since the occurrence of a variety of bone diseases are common and increasing because of the raising of the median age of the world population, the growing obesity and sedentary lifestyle lived today, plus the rising number of accidents, bone disorders are becoming a major concern. Bone disorders, whether they are caused by trauma or by a disease, like infections or tumours, affect over 20 million people annually (3,7).

In particularly, the treatment of bone cancer is extremely difficult to manage due to the huge challenge that is to repair and reconstruct the damage caused by the loss of a large part of the

bone resulting from the surgical resection of the tumour, and at the same time kill possible remain cancer cells in order to prevent a recurrence of the tumour (8,9).

### **2.2 Bone tumours: current treatment and limitations**

Although primary bone cancer is tremendously rare, being only 0.2% of all cancers (10,11), secondary bone cancer resulting from metastases of common cancers, for example from breast, prostate and lung cancer in which around 80% of patients develop bone metastases, is much more frequent and is associated with debilitating problems as pain and decreased mobility (12,13). The current clinical procedure to treat bone cancer consists in a combination of surgical resection of the tumour followed by sessions of chemotherapy and/or radiotherapy in an attempt to kill possible remaining cancer cells to avoid a relapse. The resection compromises a large part of the bone that is commonly restored with cement or bone grafts which permits the regeneration of the bone. These grafts are based in autologous bone grafts, or autografts, that are the gold standard, and in allografts (5,14,15). Autografts means that the bone grafts are removed from the patient's own body, usually from the iliac crest, skullcap, mandible or tibia. These grafts are considered the gold standard because they are biocompatible, include natural and proper growth factors and already contains own cells, which promotes osteoinduction and osteoconduction, and provide structure for the growth of bone on the surface. Allografts, which are the second most common type of bone grafts, instead of being collected from the patient himself, they are harvested from human cadavers or from living sources, such as femoral heads removed during hip replacement (5,16). Both procedures have limitations which makes them use disadvantageous. The autografts have a restricted use because of the limited number of grafts that can be taken from the patient, as well as the morbidity associated to the donor site and the need for an additional surgical site (3,14,17). On the other hand, the use of allografts eliminates some of the problems associated with autografts, but brings up other concerns, as the transmission of diseases, immunoreactions, which leads to rejection of allograft, and viral transmission. The cost and availability of both grafts are a limitation that restricts their use (14,18,19).

Coupled with the graft's issues, the chemo- and radiotherapy are not as effective as needed, for example the osteosarcoma localization is relatively avascular becoming the systemic administration of chemotherapeutics inefficient, and both therapies compromise the capability of bone to regenerate since they cause side effects on normal tissue (9,20–22).

So, due to the problems associated with these procedures, a variety of researchers are trying to overcome with other alternatives to substitute bone grafts, which are safer, less expensive and easier to use, like scaffolds made by natural and/or synthetic biomaterials (5,18,23). The main goal is to search for biocompatible materials that resembles bone and its characteristics, including provision of mechanical support and bioactivity in terms of osteogenic potential, osteoconductivity and osteoinductivity, needed for bone tissue regeneration. Being that, osteoconductivity means that material is capable of promote the recruitment and the migration of osteogenic cells into the

wound site and stimulate bone cells growth on its surface and osteoinductivity means that material is able to induce differentiation of undifferentiated cells to form osteoprogenitor cells (the stem cells of bone) once this characteristic is considered essential for successful healing large and critical sized bone defects (18,23). Aiming the substitution or at least the diminution of chemo- and radiotherapy sessions other alternatives are under investigation, as the case of hyperthermia (24). So, a combination of an innovating method capable of eliminating the remaining cancer cells (after resection of the tumour) with a biomaterial able to give support to regeneration of bone tissue, without the disadvantages of bone grafts, would be a promising advance to improve the prognosis of patients with bone tumours. Also taking into account the high probability of develop an infection resulting from the surgical procedure for the implantation of the synthetic bone graft, the addition of an antimicrobial molecule would give to this newly approach a multifaceted character reaching all the critical points of the bone cancer treatment (7,25–27).

### **2.3 Scaffolds development for bone regeneration**

#### **2.3.1 Scaffolds requirements**

Since there is a low availability of auto- and allografts and are a clear increase in bone issues with 2.2 million bone grafts used in orthopaedic procedures annually worldwide (23), plus all the disadvantages associated to those grafts mentioned earlier, researchers are developing innovating synthetic bone grafts, similar to natural bones, made of biomaterials and capable of giving support for bone regeneration. To be a synthetic alternative to natural bone, these newly bone grafts need to achieve some characteristic, as they have to be in a 3D structure, have high porosity and interconnected pores, since the living bone is a natural active 3D tissue, have to provide an appropriate environment to promote cell growth and proliferation, migration, differentiation, as well as vascularization and a suitable nutrients diffusing permitting the final goal of deposition of new bone ECM (25,28). Moreover, scaffolds need to accomplish several different biological, physical and mechanical requirements to achieve their purpose of bone regeneration:

1. they need to be biocompatible, which means that the material and its degradation products must not cause inflammatory responses neither demonstrate immunogenicity nor cytotoxicity;
2. these structures should have a controlled and adjusted biodegradability, in order to give the necessary support along time needed for bone regeneration;
3. the products of degradation must be bioresorbable;
4. they need to be highly porous structures with macro and micro porous to allow cell migration, oxygen diffusion, nutrients and waste transport and neovascularization/angiogenesis;
5. they need to be bioactive in terms of osteoconductivity and osteoinductivity to facilitate cell attachment and proliferation in the scaffold, promoting deposition of bone ECM;
6. they need to be able to provide mechanical support and have structural strength and shape, being the mechanical characteristics as similar as possible to those of bone tissue;
7. is desirable that scaffold material is easily manipulated into different shapes and sizes allowing in-situ treatment of bone defects (1,16,19,23,29).

### 2.3.2 Suitable biomaterial

There are several biomaterials that have been used for bone repair and regeneration including metals, ceramics and polymers (16). Their benefits and limitations in bone regeneration applications are summarized in Table 2.1 (16,30).

**Table 2.1** Advantages and limitations of biomaterials for bone regeneration applications (PLA: polylactic acid; PCL: polycaprolactone; PGA: poly(glycolic acid))

MATERIAL	ADVANTAGES	LIMITATIONS	EXAMPLES
<b>METALS</b>	<ul style="list-style-type: none"> <li>• Biocompatibility</li> <li>• High strength</li> <li>• Easy to fabricate and sterilizable</li> </ul>	<ul style="list-style-type: none"> <li>• Poor biodegradability</li> <li>• Need additional surgery to remove or replace</li> <li>• Potential release of toxic metal ions</li> <li>• Corrosive</li> </ul>	<ul style="list-style-type: none"> <li>• Titanium alloys</li> <li>• Stainless steel alloys</li> <li>• Gold</li> </ul>
<b>CERAMICS</b>	<ul style="list-style-type: none"> <li>• Bioactivity</li> <li>• Biocompatibility</li> <li>• Osteoconductivity</li> <li>• Osteoinductivity</li> <li>• Similar to bone components</li> <li>• Mechanically strong</li> <li>• Corrosion resistance</li> <li>• Resistance to compression</li> </ul>	<ul style="list-style-type: none"> <li>• Weakness to shearing and tensile forces</li> <li>• Brittleness</li> <li>• Degradation rates difficult to control</li> <li>• Difficult to mould</li> </ul>	<ul style="list-style-type: none"> <li>• Calcium Phosphates</li> <li>• Hydroxyapatite</li> <li>• Bioactive glass</li> </ul>
<b>POLYMERS</b>	<ul style="list-style-type: none"> <li>• Biodegradable</li> <li>• Biocompatible</li> <li>• May have biofunctional molecules on their surface</li> <li>• Can be easily modulated in different shapes</li> <li>• Low toxicity</li> <li>• Readily available</li> </ul>	<ul style="list-style-type: none"> <li>• Lack of mechanical properties for load bearing</li> <li>• May have impurities as toxins</li> <li>• Synthetic polymers are often hydrophobic and lack cell recognition sites</li> <li>• Hard to sterilize</li> <li>• Leachable in body fluids</li> </ul>	<ul style="list-style-type: none"> <li>• PLA</li> <li>• PCL</li> <li>• PGA</li> </ul>

Among all materials, biocompatible polymers meet the requirements for bone tissue engineering and their physical properties resemble the proteins of the tissues, making them materials widely used to help bone tissue regeneration. In addition, polymers have the advantages of being easily manufactured into programmed shapes and structures and can also be chemically modified or functionalized through chemical and/or biochemical reactions (1). In

comparison with ceramics and metals, polymers have the advantage that they can be built in a more customized way in terms of mechanical properties and degradation times.

There is a variety of different polymers with potential orthopaedic application. For example, polylactic acid (PLA) and polycaprolactone (PCL) are biocompatible and biodegradable and, for that, are already quite used for medical and pharmaceutical application, as implants for bone regeneration and as drug delivery systems. Both suffer hydrolysis *in vivo*, being eliminated through excretory pathways (16,31). Beside PLA and PCL, there are other synthetic degradable polymers used for orthopaedic applications, as poly(glycolic acid) (PGA), poly(ethylene glycol) (PEG) and poly(lactic-co-glycolic acid) (PLGA), that are, as PLA and PCL, approved by the Food and Drug Administration (FDA) for human use in medical devices (1,16). Polymers derived from lactic acid have been widely adapted in biomedical field because of their versatility and relatively low-cost, so PLA being an environment friendly material that can be produced using natural sources, with a high mechanical strength and well known biocompatible and biodegradable properties, makes it a promising material to produce scaffolds for bone regeneration. In addition, there are only few reported cases that indicate adverse effects of PLA in patients (16,30,32,33). Because of that, PLA was the chosen material to produce scaffolds in the present work.

### **2.3.3 Fabrication method**

Native bone is a natural and complex 3D structure that is provided by ECM allowing the support for spatial organization of the tissue and cell anchorage and proliferation, therefore a 3D structure is a demand to apply in bone regeneration.

There are several techniques to fabricate 3D porous structures, from the traditional ones, that includes solvent casting, polyurethane foam, phase separation, freeze drying, among others, to the modern ones, as 3D printing, that have been developed with the progress of technology. With the conventional techniques, it is difficult to achieve a well-defined architecture with a precisely control of the pore size, pore interconnection and total porosity, what causes 3D printing technique to be the most promising modern technique for scaffolds fabrication. 3D printing method overhaul these issues, being able to produce a pre-determined and well-defined structure with a controlled pore size, also permits repeatability and the elimination of organic solvents used in conventional methods that may be toxic or damaging for cells (9,16,28,34,35).

3D printing, or additive manufacturing, is based on the design of scaffolds with the desired geometry and porosity with computer assisted design (CAD), imported into a slicing software and printed with a 3D printing machine that adds material in a continuous layer by layer deposition, through computer assisted manufacturing (CAM), until achieve the final shape of the scaffold. This modern technique has a significant advantage for bone-graft fabrication: it permits to be patient-specific. 3D printing allows the preparation of customized implants with precisely controlled architectures for geometrically complex bone defects (resulting from tumour resection) and controlled size, shape and porous dimensions, since it is possible to design and print the scaffold with CAD/CAM through converting computerized tomography (CT) and/or magnetic

resonance imaging (MRI) of clinical defects into CAD models, making the implants customized for the patient defect (9,16,28,30,34,35). There are several authors in literature that present 3D printed scaffolds to apply in bone tissue engineering as is the case of Zhang J. et al., Ma H. et al., Ritz U. et al., among others (8,9,36).

There are different 3D printing processes that have been used to produce scaffolds that aim bone tissue regeneration as stereolithography (SLA), one of the earliest 3D printing developed techniques, selective laser sintering (SLS), fused deposition modelling (FDM), among others. Between them, FDM is the most commonly used and inexpensive additive manufacturing technique and is based in the passage of a thermoplastic filament into a temperature-controlled heating chamber who melts the filament, which is then extruded through a nozzle onto the platform where is precisely deposited it in a layer-by-layer fashion until the object is formed. The molten filaments cool down allowing them to fuse together rapidly creating a scaffold (16,30,35). Since FDM is a 3D printing method successfully adapted to the production of synthetic scaffolds for bone regeneration, it is cost effective, simple and high speed, as well as already been successfully used to print PLA scaffolds (16,35), it was selected for the production of scaffolds in the present work.

### **2.4 Enhance osteogenic potential of PLA**

PLA, as other polymers, has a lack of tissue-material interface properties (i.e. bioactivity) and has low osteoinductive and osteoconductive properties that need to be overtaken. A commonly way to surpass these problems is combining the properties of inorganic materials, especially calcium-based ceramics, with the properties of polymers (14,16,18,33). Calcium-based ceramics are, among others, calcium phosphates (CaP) salts of which hydroxyapatite (HA), dicalcium phosphate (DCP) and tricalcium phosphate (TCP) make part of. These CaP have excellent osteoinduction potential, since their *in vivo* degradation produces calcium and phosphate ions that promotes new bone formation, have good osteoconductive properties, are very similar in structure and chemical composition to the mineral content of native bone and are biocompatible, facilitating the integration with host tissue. Because of these characteristics, ceramics have been used since the 70's to produce scaffolds for bone regeneration, but once they are often fragile, have low porosity, intrinsic brittleness and high crystallinity, limits their use alone as bone grafts. Alternatively, it has been used in a combination with polymeric scaffolds optimizing the physiochemical and biological properties to achieve a better perspective for bone regeneration (6,14,16,18). Among the CaP available, hydroxyapatite (HA) is a good option once it has excellent properties for bone regeneration. HA is the natural main building block of bones, is biocompatible, has a slow biodegradation rate, lack of cytotoxicity, is non-inflammatory and has a unique mechanical stability. It also can stimulate the expression of osteogenic growth factors such bone morphogenic proteins (BMP) and promote alkaline phosphate (ALP) activity in mesenchymal stem cells (MSCs) (16,37).

Different researchers have shown that nanoscale ceramics have advantages in bone regeneration over micron sized ceramics. When nanometer grain size ceramics are present in the scaffolds for bone regeneration, the osteoblast adhesion and subsequent mineral deposition is greatest when compared to conventional size ceramics. Nanoscale ceramics, beyond the biocompatibility improvement, also enhance mechanical properties of the polymeric scaffold, making HA nanoparticles (nHA) a better option (1,18). Combining PLA scaffolds with nHA is a promising strategy that fulfil the requirements to use as substrate for bone regeneration and increases the compression strength of PLA scaffold. However, must be taken in account that the rate of degradation of PLA/nHA scaffolds become reduced, mainly because of the buffering effect of the ceramic that difficult the autocatalytic degradation of the polymer (18).

The use of ceramics combined with PLA has as the main goal to increase osteogenic capacity and trigger biomineralization helping the bond between material and bone tissue. Consequently, PLA loaded with nHA appears to be a good approach to the present work.

### **2.5 Hyperthermia and Superparamagnetic iron oxide nanoparticles (SPIONs)**

In order to ensure that there will be no relapse due to remaining cancer cells, it is needed an innovating method combined with the scaffold to eliminate cancer cells, after surgery, to avoid chemo- and radiotherapy.

A promising cancer treatment technique is hyperthermia. First applied in the beginning of 20<sup>th</sup> century, from that time until now has gained an increase interest due to its advantages over chemo- and radiotherapy, once these two are associated with a debilitating state of the patient submitted to those therapies and are unable to completely eliminate tumour cells. Hyperthermia approach permits killing cancer cells in a short period of time without affect the healthy ones (22,38), which is an important feature in the case of bone cancer allowing to kill the remain cancer cells without putting in risk the regenerative capacity of healthy bone tissue.

Hyperthermia, or thermal therapy, consists on the increase of tumours' temperature with respect to standard temperature of the human body, to temperatures between 40 and 45°C (these temperatures differ between authors), through the heat transferred within cells from a heated environment (39,40). The hyperthermia effect is more pronounced in tumour cells because these cells have a higher metabolism than normal tissue making cancer cells more responsive to any change in surrounding temperature and pH, also they contain many somatic mutations which makes them much more prone to the increase of temperature that activates numerous pathways that lead to cell death (15,41). This local heated environment can be reached through various techniques according to the site of the tumour. For example, hyperthermia can be based on microwaves, radiofrequency energy and ultrasounds applied at superficial tumours and photothermal therapy, or infrared radiation, and magnetic hyperthermia for no superficial tumours. Magnetic hyperthermia is the most studied for medical applications and the one with best results in terms of efficiency (9,22,38,40). Also, magnetic hyperthermia, beyond the killing effect on

cancer cells, is also being considered a promising treatment in bone diseases, because it is being reported that weak magnetic fields may stimulate the proliferation and the differentiation of osteoblasts and promote the expression of growth factors, as BMPs, which accelerates the regeneration process promoting bone healing, increasing the osteointegration of implants by encouraging the bone growth along the implants and increasing bone density and calcium content (4,42–44).

Magnetic hyperthermia was officially introduced to clinical practice in 2011, as a combined treatment for glioblastoma, and it is based on magnetic nanoparticles (MNPs) that are subjected to an external alternating magnetic field (AMF) of appropriate frequency and amplitude, which is responsible for oscillate the magnetic moment of each particle converting magnetic energy into heat, known as Brownian and Neel relaxation process (38,41,42). The treatment efficiency, with the aim of a lethal effect over cancer cells, depends on the temperature reached, the exposure time to heat and the type of cancer cells (40).

MNPs have a variety of biomedical and clinical applications and are promising materials for magnetic hyperthermia agents once they acquire superparamagnetic properties at diameters between 10 and 100 nm, what means that these nanoparticles do not retain any magnetism after removal of the magnetic field applied, which is a great advantage for magnetic hyperthermia application (1,37,41,45). This happens based on Brown and Neel relaxations mechanism, which is the rotation of magnetic moments of the nanoparticles along with the external alternating magnetic field (44,46). Beyond superparamagnetism, MNPs have other advantages as low cytotoxicity, biocompatibility and biodegradability. Although promising, they also have some drawbacks, namely poor chemical stability, high aggregation propensity, low adsorption drug capacity, poor release rate and short retention time in the blood stream, drawbacks that can be overcome by being associated with the PLA and nHA. Adding the fact that these scaffolds are looking to promote bone formation, it is known that the internalization of magnetic nanoparticles modulate intracellular signalling pathways stimulating MSCs to differentiate in osteogenic ones (37).

A variety of MNPs with different properties and morphological structures have been studied for medical applications in bone regeneration, among them are transition metals as iron (Fe) and copper (Cu) and metal oxides, essentially iron oxide as magnetite ( $\text{Fe}_3\text{O}_4$ ), the most common, maghemite ( $\gamma\text{-Fe}_2\text{O}_3$ ) and hematite ( $\alpha\text{-Fe}_2\text{O}_3$ ) (1,43,47). Particularly, superparamagnetic iron oxide nanoparticles (SPIONs), that can be magnetite or maghemite, have been recognised as a promising material for magnetic hyperthermia and for other medical applications, as bone tissue repair, for diagnose techniques and for drug delivery, essentially because of their proven biocompatibility (1,41,42,47,48). Furthermore, SPIONs are biodegradable *in vivo*, can be easily cleared from the body through renal and biliary excretions and are small enough to evade the reticuloendothelial clearance system of the body and to enter capillaries/cells within the body tissues. After inside the cells, SPIONs are internalized in lysosomes where it is presumed to occur degradation into iron ions. Nevertheless, the toxic effect of these nanoparticles as to be

considered and depends on a variety of factors, such as the number of particles used and their physico-chemical properties (1,49–51).

Cancer cells have an elevated rate of ROS in a delicate balance with a variety of antioxidant proteins and SPIONs act against cancer cells by disrupting this redox homeostasis, which leads to the selective tumour cell toxicity. SPIONs induce cytotoxicity, after cell internalization, potential by releasing iron ions into the cytoplasm where they participate in the Haber-Weiss chemistry through the Fenton Reaction catalysing the formation of ROS, as hydrogen peroxide, hydroxyl radicals and superoxide anions, causing oxidative stress that results in the disrupted redox homeostasis and consequently in rapid lipid oxidation and protein and DNA damage, leading to cancer cell death. In normal conditions, intracellular iron ions bind to specific proteins and just a small amount of iron ions are available for Fenton reaction (8,37,52). Even more, and as mentioned earlier, when applying an alternating magnetic field over SPIONs they are heated up, due to Néel and Brownian relaxations, making the target tissues reach temperatures between 40 and 45 °C. At these temperatures, cancer cells are injured or killed owing to haemorrhage, stasis and vascular occlusion, but normal cells support the heat and survive (9).

In the case of bone tissue regeneration, SPIONs have the advantage of, even without external magnetic field, exhibiting osteoinductive properties promoting bone regeneration. It is known that they are not toxic to human MSCs, but instead they promote cell growth, cell proliferation, stimulate ALP activity (a measure of osteogenic differentiation) and the expression of osteogenic related genes (9,51,53). As seen in Zhang, J. et al. research, MSCs cultured in scaffolds with SPIONs showed a better attachment and proliferation when compared to cells cultured in scaffolds without SPIONs (9). This occurs because SPIONs diminish intracellular H<sub>2</sub>O<sub>2</sub> through the intrinsic peroxidase-like activity of magnetic nanoparticles that catalyse the breakdown of H<sub>2</sub>O<sub>2</sub>, promoting cell growth and accelerating cell cycle progression by the free iron ions released from lysosomal degradation (9,51).

All these characteristics of SPIONs make them a promising approach for use as hyperthermia agent to target and remain cancer cells after ablation of bone tumour and with the regenerative purpose in mind. For these reasons, in the present study, PLA scaffolds will be also loaded with SPIONs aiming a local delivery to the desired target.

### 2.6 Prevention of bone infection

The resection of the tumour and the replacement of the defected bone implies a surgical step that brings concerns, namely the emergence of inflammation and infection that should be immediately treated to prevent the biofilm formation that can spread to healthy bone and compromise all the healing process, in particular by *Staphylococcus aureus*, a major pathogen in bone associated infections due to its ability to adhere and form biofilms on implants and bones. To address this issue, the conventional method is the systemic administration of antibiotics, including tetracycline (TC) antibiotics, however this type of administration is not as effective as necessary and may lead to side effects including development of antibiotic resistance, destruction

of beneficial flora and toxicity and nephrotoxicity caused by the high dosage of antibiotics (7,25,54). A local controlled delivery system of TC can be an effective strategy to surpass the conventional methods.

TC antibiotics have a broad antibacterial spectrum being effective against gram-positive and gram-negative bacteria, including minocycline (MH). MH is a semi-synthetic tetracycline, used for over 30 years, that inhibits bacterial protein synthesis with proved antimicrobial activity against *S. aureus* by several authors (25,55). Additionally, MH has anti-inflammatory activity and osteoinductive properties that positively stimulates bone metabolism, which results in the improvement of bone tissue remodelling and healing. MH enhance bone formation by increase osteoblastic activation, inhibit the osteoclast bone resorption, up regulate protein synthesis, enhance the differentiation process of osteoprogenitor cells and stimulates mineral deposition (5,55). The combination of MH with PLA scaffolds has already been shown as a good approach to avoid implant/bone infections by the local delivery of antibiotic with the additional advantage of osteoinductive properties necessary for bone regeneration (25).

SPIONs mentioned earlier, for use in magnetic hyperthermia, were also found to be good inhibitors for different bacterial strains, actually Ismail R. et al. demonstrated the effective antimicrobial activity of iron oxide nanoparticles (IONPs) against *S. aureus* and Thukkaram, M. et al. they antibiofilm properties (56,57). IONPs interact with bacteria cell membranes by electrostatic interaction damaging the bacterial membrane and inducing oxidative stress by ROS formation, however the antimicrobial activity of IONPs seems to depend on the size, on physicochemical properties and on the concentrations of the nanoparticles (56,58). So, the presence of SPIONs in scaffolds can further enhance antimicrobial properties to avoid infection.

### 2.7 Cellular assays on PLA scaffolds

When developing a device for biomedical applications it is important to evaluate their functionality, biocompatibility and bioactivity, to evaluate if this newly device is producing harmful effects on the surrounding tissue of implantation. In the case of scaffolds for bone tissue engineering, is also essential to appraise if it achieves effective bone remodelling and fracture healing, once it is required for the scaffold to replicate the functionality of natural bone extracellular matrix, interact with host tissue, promote cell attachment and tissue growth and be biodegradable with degradation products that produce minimal immune reaction. To prove if the scaffolds accomplish this requests, pre-clinical trials, as *in vitro* and *in vivo* experiments, should be performed (28,59,60).

The cells used to perform *in vitro* assays need to be chosen according to the target tissue to where scaffolds were idealized. In the case of bone tissue, one of the most used cell lines is the MG-63 human osteoblast-like cells, an adherent cell line originally derived from a human osteosarcoma.

### **2.7.1 Cytocompatibility evaluation**

The first experiments to be performed to evaluate the biocompatibility of biomedical devices are the *in vitro* ones and are the ones that will be performed in the present work. For *in vitro* tests, it is used cell cultures where it is placed the scaffolds in direct or indirect contact with the cell cultures. After a period, the existence or absence of cytocompatibility is assessed through the observation of occurrence or non-occurrence of morphological alterations in the cells and through the assessment of cellular viability, if cells are dead or alive, through a set of assays (28,59).

In particularly, cell viability and cell proliferation assays are used to determine, in a quantitative way, the cytocompatibility of the scaffolds and other medical devices. Tetrazolium salts reduction, in which the most frequently used is the MTT (3-[4,5-dimethylthiazol-2-yl]-2,5-diphenyltetrazolium bromide; thiazolyl blue tetrazolium bromide) assay, where the yellow MTT solution, is reduced by mitochondrial dehydrogenases from the metabolically active cells to a purple formazan and its absorbance read (14,53,59,60), is one of the quantitative cell viability assays.

AlamarBlue assay, another quantitative assay, is used to study the cell viability through metabolic activity of cells, monitoring the reducing environment of the living cell. Cells metabolic active produce a reducing environment what causes the reduction of resazurin, the non-fluorescent blue dye present in the AlamarBlue solution, into the highly fluorescent pink/red resorufin (fluorescent signals are measured through a fluorescent reader at an excitation wavelength at 530-560 nm and an emission wavelength at 590 nm). Resazurin is non-toxic and permeable through cell membranes that acts as an intermediate electron acceptor in the electron transport chain without interfering with the normal transfer of electrons, which by accepting the electrons changes from the oxidized state to the reduced one (61,62). Since resazurin is a non-toxic reagent, permits to measure the cell viability over the weeks and follow the cell proliferation rate.

Another assay that permits to evaluate cell death is the propidium iodide (PI) uptake test, in which the loss of plasma membrane integrity, a common event in all forms of cell death, allows the enter of the membrane-impermeable dye PI into the cells, which will bind to DNA and stain the death cell. The stained cells may be counted through flow cytometry, visualized on microscope or quantitatively measured through a fluorescent reader (63).

Between others, these are some of the assays that can be performed to assess biocompatibility of the newly scaffolds.

### **2.7.2 Evaluation of osteogenic potential**

Scaffolds developed at the present work have as one of the main goals stimulate the proliferation and differentiation into bone cells to achieve bone tissue regeneration. So, it should be performed *in vitro* and *in vivo* tests to assess scaffolds' osteogenic capacity through the analysis of characteristic elements of bone formation. One characteristic that identifies bone formation is the activity of alkaline phosphatase (ALP) enzyme by osteoblast cells that can be

measured by the ALP activity. ALP activity is a marker for earlier osteoblastic differentiation, meaning that higher ALP levels more osteoblast cells are present (14,17,64). Mineralization and ECM formation is another characteristic of bone formation that can be qualitatively and/or quantitatively measured through the Alizarin Red Stain assay, which is based on the staining of calcium rich deposits, characteristics from ECM deposition, present in the surface of scaffolds followed by microscopic observation or absorbance measure (9,60).

Another indicative of osteogenic capacity is the scaffolds bioactivity potential, characterized by the formation of a bone-like apatite layer formed by the deposition of calcium phosphates (biomineralization) on the biomaterial surface. This apatite layer allows the biomaterial to form stronger bonds with the bone promoting a proper integration with the minimum formation of surrounding fibrous tissue (15,65). This characteristic can be predicted by immersing the scaffolds in simulated body fluid (SBF), that has ion concentrations identical to those of human blood plasma, or in cell culture medium and analyse the formation of apatite on scaffolds' surface (65,66). If a scaffold is cable of promoting the biomineralization process in contact with SBF and/or cell culture medium it will be called bioactive and have a higher potential of, *in vivo*, positively regulate cell and bone tissue response promoting a better integration in the organism (33).



# 3 Materials and methods

## 3.1 Materials

Poly(lactic acid) (PLA) for scaffold production was purchased in filament form from Real PLA and the materials for scaffolds' adsorption were collagen hydrolysate type I fibrillar, pleasantly donated by Dra. Mădălina Kaya from Department of Collagen Research (Romania), hydroxyapatite nanoparticles (nHA) and superparamagnetic iron oxide nanoparticles (SPIONs), donated by Professor Catarina Santos from Instituto Politécnico de Setúbal, and minocycline hydrochloride, kindly offered by Atral Cipan (Portugal).

## 3.2 Cell culture

The human osteoblast cell line MG-63 (ATCC®CRL-1427™), derived from a human osteosarcoma, was obtained from the American Type Culture Collection (ATCC). The cells were seeded in culture flasks with RPMI 1640 Medium (Gibco, ThermoFisher) supplemented with 10% fetal bovine serum (Gibco, ThermoFisher), antibiotics (Gibco, ThermoFisher): 100 µg/mL streptomycin and 100 U/mL penicillin; and with 2mM of the aminoacid L-glutamine (Life Technologies) and incubated at 37°C in a 5% CO<sub>2</sub> atmosphere. The medium was changed twice a week, and, at the confluence of 80-90%, cells were trypsinized with TrypLe express (Gibco, Thermo Fisher), a set of trypsin-like enzymes, and proceeded to the passage of cells.

In the needed cases, cells were quantified using a haemocytometer and the Trypan Blue (Sigma Aldrich) exclusion test. For that, cells were trypsinized and a volume of 20 µL of cells was removed and added equal volume of Trypan Blue (dilution factor = 2). After the coverslip is on the haemocytometer, both chambers were filled with the cells suspension and the viable cells were counted in the main square of the grid through an inverted microscope (MEIJI). Concentration of viable cells were calculated through the equation:

$$\text{Number cells/mL} = \text{Number viable cells} \times 2 (\text{Dilution factor}) \times 10^4$$

### 3.3 SPIONs fundamental characterization

#### 3.3.1 Zeta potential of SPIONs

Surface charge of the SPIONs was analysed in different media and measured by electrophoretic light scattering using a Zetasizer Nanoseries Nano Z from Malvern Instruments. Different tested media were: i) filtered 0.22 µm purified water; ii) PBS 10mM (Sigma-Aldrich) pH 7.4, corresponding to the physiological pH and pH 6.5, corresponding to the infection pH, iii) RPMI 1640 medium (Gibco, Thermo Fisher), a complete culture medium; and iv) Brain Heart Infusion (BHI) medium (Biokar Diagnostics) with glucose at 1% (w/V).

#### 3.3.2 *In vitro* evaluation of SPIONs oxidative stress

Intracellular reactive oxygen species (ROS) production, when cells were in contact with SPIONs, was measured using a peroxidase-sensitive fluorescent probe: 2,7'-dichlorodihydrofluorescein diacetate (H2-DCFDA, Thermo Fisher Scientific). MG-63 cells at a density of  $2 \times 10^5$  cells per well in a 96-well plate were incubated for 24 h at 37°C in 5% CO<sub>2</sub> humid atmosphere. Then, cells were incubated for 30 min with 20 µM of H2-DCFDA at the same conditions as before and after the probe loading into the cell, the excess was removed, and fresh medium was added. Cells were incubated with different concentrations of SPIONs (1, 0.5 and 0.25 mg/mL) at 37°C in 5% CO<sub>2</sub> humid atmosphere. After predefined time points (3 h, 6 h and 24 h), the fluorescence at wavelengths excitation at 485 nm and emission at 520 nm from each well was measured using a microplate reader (FLUOstar Omega, BMG Labtech). A group of cells was maintained untreated as a negative control, 500 µM of H<sub>2</sub>O<sub>2</sub> was used as a positive control and 1 mg/mL of ascorbic acid was used to validate the assay.

#### 3.3.3 *In vitro* evaluation of SPIONs cytotoxicity

*In vitro* cytotoxicity of SPIONs was investigated on MG-63 cells by staining the dead cells through the propidium iodide (PI) assay and by identifying the live ones through the AlamarBlue and MTT assays. To carry out these assays, cells were placed at a density of  $2 \times 10^5$  cells per well in a 96-well plate and incubated for 24 h at 37°C in 5% CO<sub>2</sub> humid atmosphere. Different concentrations of SPIONs (1, 0.5 and 0.25 mg/mL) and sodium dodecyl sulphate at 1 mg/mL (SDS, AppliChem), for positive control, were added to the wells and were incubated for more 24 h at the same condition as before. A set of wells was maintained with cells untreated, without adding SPIONs or SDS.

After the 24 h, the PI assay was performed by adding 0.3 mM propidium iodide (Sigma Aldrich) in each well and immediately measured the fluorescence (excitation: 485 nm; emission: 590 nm). Next, the AlamarBlue assay was performed by adding 10 µl of AlamarBlue solution (Sigma Aldrich) in each well, incubated for 2 h at 37°C in 5% CO<sub>2</sub> humid atmosphere and fluorescence was measured (excitation at 540 nm and emission at 590 nm). The last assay to be

performed was the MTT assay in which was added MTT solution (0.25 mg/mL, Sigma Aldrich) in each well and incubated for 2 h at 37°C in 5% CO<sub>2</sub> humid atmosphere. After incubation, the excess reagent was removed, 100 µl of DMSO (VWR Chemicals, Prolabo) was added and the 96-well plate was placed at 200 rpm agitation plate (LD-40, Labinco) for 15 min to solubilize the crystals formed by the MTT reaction. After 15 min, the absorbance was measured at 570 nm. The values of fluorescence and absorbance were measured using a microplate reader (FLUOstar Omega, BMG Labtech).

#### **3.3.4 SPIONs cellular uptake study**

MG-63 cells were seeded at a cell density of  $2 \times 10^5$  cells/mL on top of round glass slides in a 24-well plate in RPMI 1640 medium for 24 h at 37°C in 5% CO<sub>2</sub> humid atmosphere. The SPIONs were added to the attached cells in two different concentrations and incubated for two different periods of time, namely: 0.5 and 1 mg/mL incubated for 1 h (C1t1 and C2t1, respectively) and 0.5 and 1 mg/mL incubated for 14 h (C1t2 and C2t2, respectively). Cells incubated without SPIONs were used as a control group. After incubation, the cells were washed 3 times with PBS (Sigma-Aldrich) + 20 mM glycine (BioRAD) solution and cells were fixed with 4% paraformaldehyde (Sigma Aldrich) for 10-15 min at room temperature (RT) and washed again 3 times with the same solution. With the aim of observe the SPIONs cellular internalization through fluorescent microscopy, cells were permeabilized with 0.1% Triton X-100 solution (Sigma Aldrich), washed 3 times with PBS+20 mM glycine solution and the actin marker, phalloidin-TRITC (Thermo Fisher Scientific), was added and incubated at RT for 30 min cover from the light. After incubation with the marker, the washing process with PBS+20 mM glycine solution was repeated. Finally, the slides with the fixed cells were mounted over a drop of microscope preparation with DAPI (ProLong Gold Antifade Mountant with DAPI, Invitrogen, Thermo Fisher Scientific) on a blade and their fluorescence was observed and recorded on an Axioscop 40 fluorescence microscope with an AxioCam HRc camera (Carl Zeiss). Images were processed with AxioVision software (Rel. 4.8.1, Carl Zeiss).

### **3.4 Preparation and functionalization of PLA scaffolds**

3D PLA scaffolds were printed through fuse deposition modelling (FDM) process (BQ Prusa i3 Hephestos) by the extrusion of a PLA filament with 1.75 mm of diameter, as in Martin V. et al. (25).

#### **3.4.1 Surface treatment**

3D PLA scaffolds were submitted to alkali hydrolysis treatment as described by Guo C. et al. (39), aiming the improvement of PLA surface hydrophilicity and roughness needed to a superior cell adhesion. For that, scaffolds were first immersed into the alkaline hydrolysis solution,

composed by ethanol 96% (V/V) (Carlo Erba) with sodium hydroxide (NaOH) 0.25 M (Akzo Nobel) at a volume ratio of 1:1, for 4 h at RT in 220 rpm agitation on a mixing plate (LD-45, Labinco). After this period, PLA scaffolds were subjected to a washing step with citric acid 0.5% (w/V) (Merk) followed by deionized water. This process can be seen in the diagram of the Figure 3.1.

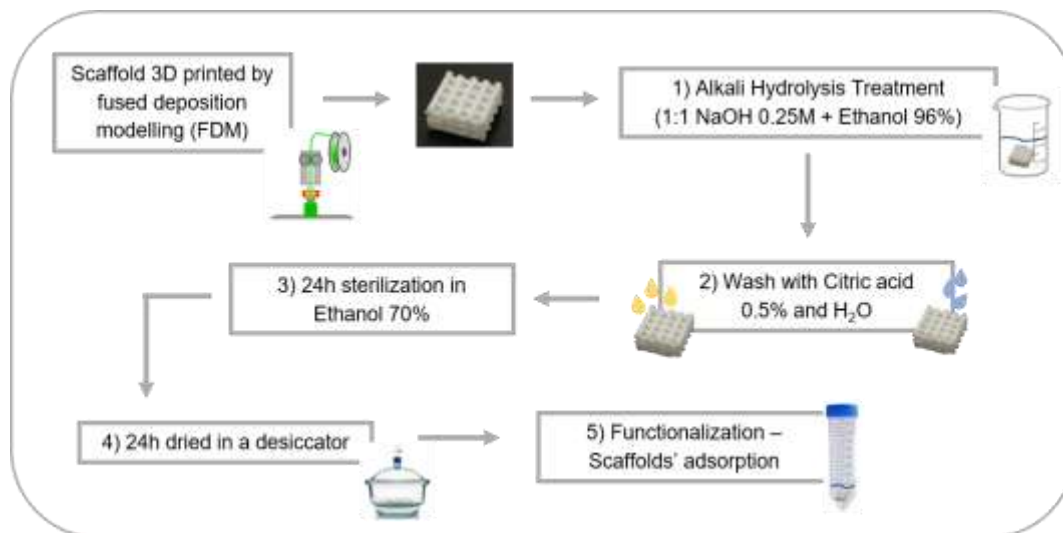


**Figure 3.1** Schematic representation of scaffolds preparation: Surface treatment and functionalization

### 3.4.2 Functionalization

After surface treatment, PLA scaffolds were sterilized by immersion into ethanol 70% (V/V) (Merck) solution in 300 rpm agitation plate (LD-40, Labinco) for 24 h and dried in a desiccator for more 24 h (Fig. 3.1). Further, PLA scaffolds were functionalized (Fig. 3.1) with different combination of collagen (Col), hydroxyapatite nanoparticles (nHA), superparamagnetic iron oxide nanoparticles (SPIONs) and minocycline (MH) according to Table 3.1.

**Table 3.1** Groups of scaffolds according to the surface functionalization

Group 1 (G1)	PLA + Col (5 mg/mL)
Group 2 (G2)	PLA + Col (5 mg/mL) + nHA (5 mg/mL)
Group 3 (G3)	PLA + Col (5 mg/mL) + SPIONs (1 mg/mL)
Group 4 (G4)	PLA + Col (5 mg/mL) + nHA (5 mg/mL) + SPIONs (1 mg/mL)
Group 5 (G5)	PLA + Col (5 mg/mL) + nHA (5 mg/mL) + SPIONs (1 mg/mL) + MH (0.5 mg/mL)

Pre-prepared solution of Col and MH were filtered through a sterile 0.2  $\mu\text{m}$  pore size filter (PES filter, Filtrés Fioroni) with the purpose of sterilizing. The nHA and the SPIONs were added, in the groups needed, to the Col and MH prepared solutions to make a final concentration of 5

mg/mL and 1 mg/mL, respectively. The SPIONs concentration of 1 mg/mL was settle based on Sneha M. et al. (38) and through the results of SPIONs cytotoxicity assay accomplished in the present work. PLA scaffolds were immersed into the according solution (Table 3.1) and the adsorption was performed at RT, in rotative agitator (VWR) for 24 h. After 24 h adsorption period, scaffolds were dried in a desiccator for at least 48 h.

## 3.5 Characterization of PLA scaffolds

### 3.5.1 Morphological and chemical characterization

The morphological analysis of PLA scaffolds surface was carried out by scanning electron microscopy (SEM) using a JEOL JSM-7001F equipment, with an energy beam of 15 kV, and the analysis of the elemental chemical composition was conducted by the respective X-ray energy dispersive spectrometer (EDS). Once PLA is not a conductive material, the samples were coated with a thin layer of conductive mixture of gold (Au) and palladium (Pd) to increase the conductivity of samples and make them proper for SEM and EDS analysis.

### 3.5.2 Swelling behaviour

The *in vitro* swelling characterization of PLA scaffolds was performed weighting the dry scaffolds and subsequently immersing them in HEPES solution (10 mM pH 7.4, VWR Chemicals) at 37°C (Memmert incubator) in 250 rpm agitation plate (LD-40, Labinco), for pre-determined periods of time. At each time set, the scaffolds were removed from the solution, the excess solution was slightly dried, and the scaffolds weighed. The procedure was done in triplicate and the swelling percentage was determined based on the following formula:

$$\text{Swelling (\%)} = \frac{(W_f - W_o)}{W_o} \times 100$$

Where  $W_f$  is the scaffold's weight measure at a certain time and  $W_o$  is the scaffold's dried weight (67–69).

In this assay, two additionally groups of scaffolds were also characterized, namely the PLA without alkali hydrolysis treatment and the PLA with alkali hydrolysis treatment, with the aim of analyse the influence of the alkali hydrolysis treatment in the swelling capacity of the scaffolds.

### 3.5.3 *In vitro* minocycline release study

The MH release profile of PLA scaffolds was analysed through the G5: PLA-Col-nHA-SPIONs-MH). For that, specimens from that group (n=3) were incubated with 3 mL of HEPES buffer (VWR chemicals) 10 mM at pH 7.4 at 37°C in 250 rpm mixing plate (LD-40, Labinco). Scaffolds from G4: PLA-Col-nHA-SPIONs were subjected to the same treatment as a blank. At

predetermined period of times, throughout a 28 h period, 1 mL of the supernatant was collected and analysed in triplicate to determine the minocycline content using a microplate reader for UV detection at 350 nm (FLUOstar Omega, BMG Labtech). The volume of supernatant removed was replaced with equal volume of HEPES.

### 3.5.4 *In vitro* bioactivity study

*In vitro* bioactivity studies of samples from the 5 groups were performed by soaking the samples in Simulated Body Fluid (SBF) with ion concentrations similar to those in human blood plasma, and in RPMI 1640 complete culture medium (Gibco, ThermoFisher). The SBF solution was prepared as in Kokubo T. et al. (65) with some changes based on the available chemical compounds, the chemical composition of it is described in Table 3.2. The procedure for *in vitro* bioactivity studies was followed as explained in Kokubo T. et al. and in Farzin A. et al. (15,65), where four samples of each group were immersed in 3 mL of SBF or RPMI 1640 medium inside a 50 mL falcon tube and maintained in a water bath (Mettler), at 37°C with light shaking. A sample of each group was removed per week in a total period of 28 days (4 weeks), and the samples removed were gently rinsed with distilled water and dried at RT in a desiccator. The formation of a bone-like apatite layer in the scaffolds surface was analysed through Attenuated Total Reflection Fourier-transform Infrared Spectroscopy (ATR-FTIR, Nicolet 5700, Thermo Electron Corporation) analysis and through SEM equipped with EDS (JSM7001F JEOL equipment) with an energy beam of 20 kV. PLA scaffolds are not conductive, so the samples were coated with a conductive mixture of gold (Au) and palladium (Pd) to increase the conductivity of the samples to make them proper for SEM and EDS analysis.

The SBF solution and the culture medium, after removing the samples, were studied for changes in pH using a pH meter (inoLab 730, WTW).

**Table 3.2** Chemical composition of simulated body fluid (SBF)

Reagent	Amount in 200 mL of distilled water
NaCl (AppliChem, GmbH)	1.607 g
NaHCO <sub>3</sub> (Sigma-Aldrich)	0.071 g
KCl (Merck)	0.045 g
K <sub>2</sub> HPO <sub>4</sub> (Merck)	0.035 g
MgCl <sub>2</sub> .6H <sub>2</sub> O (AppliChem, GmbH)	0.062 g
1.0M – HCl (AppliChem, GmbH)	7.8 mL
CaCl <sub>2</sub> .2H <sub>2</sub> O (Merck)	0.077 g
Na <sub>2</sub> SO <sub>4</sub> (Merck)	0.014 g
Tris (AppliChem, GmbH)	1.224 g

### 3.6 Microbiological studies: evaluation of the antimicrobial activity

The microbiological assays were performed using *Staphylococcus aureus* ATCC 25923, obtained from American Type Culture Collection, cultured in Tryptic Soy Agar (TSA) for 24 h at 37°C.

#### 3.6.1 Agar diffusion assay

The agar diffusion assay was conducted to evaluate the antimicrobial activity of the scaffolds. *S. aureus* inoculum was prepared following the guidelines of the Clinical and Laboratory Standards Institute (CLSI) (70). In short, isolated colonies of the bacteria were mixed into Mueller Hinton Broth (Biokar Diagnostics) culture medium and diluted until achieve 0.5 McFarland units, which correspond to  $1 \times 10^8$  CFU/mL, at a wavelength of 600 nm using a spectrophotometer (U-2000, Hitachi). After achieving the right concentration of bacteria in suspension, the inoculum was spread on Muller Hinton Agar (Biokar Diagnostics) plates. The tested scaffolds were placed in the plate, as well as the two 6 mm filter disks, one containing 10  $\mu$ L of distilled water (negative control) and the other containing 10  $\mu$ L of MH at 3 mg/mL (positive control). The petri dishes prepared were incubated (Ultima, Revco incubator) at 37°C for 24 h. Passed the period of incubation, the diameter of the inhibition zones of the samples and the controls were measured three times each with a digital Vernier calliper. The agar diffusion assay was performed three times in independent experiments, as in Martin V. et al. (25).

#### 3.6.2 Biofilm inhibition assay

The evaluation of scaffolds' capacity to inhibit the formation of biofilm was performed fixing the scaffolds at the bottom of the wells in a 24 well plate under aseptic condition. Isolated colonies of *S. aureus* were suspended in Brain Heart Infusion (BHI) medium (Biokar Diagnostics) with glucose at 1% (w/V), adjust to  $3 \times 10^8$  CFU/mL and then diluted to achieve a final concentration of  $3 \times 10^6$  CFU/mL. The inoculum with the final concentration was placed in each well with the scaffold. In wells with the scaffold used as negative controls, was only placed BHI medium, without the bacteria. The 24 well plate was incubated at 37°C (Ultima, Revco incubator) for 24 h. After, samples were washed twice with PBS and the biofilm was fixed with ethanol solution in gradual percentages, 75% for 10 min, 90% for 10 min and 96% for 20 min. The evaluation of the presence of biofilm in the scaffolds was performed through SEM analysis (JSM7001F JEOL) with an energy beam of 10 kV. PLA scaffolds are not conductive, so the samples were coated with a conductive mixture of gold (Au) and palladium (Pd) to increase the conductivity of the samples to make them proper for SEM analysis.

### **3.7 *In vitro* cellular studies**

#### **3.7.1 Cytocompatibility and cell proliferation**

The proliferation of MG-63 cell culture on the scaffolds' surface was assessed by monitoring the metabolic activity of cells using the non-toxic AlamarBlue assay (61,71) with the aim of knowing if PLA scaffolds under study are cytotoxic or not. AlamarBlue assay is based on the reduction of resazurin into resorufin, which has a red colour and high fluorescence, by metabolically active cells (72). Briefly, to perform this assay,  $2 \times 10^5$  cells/mL were seeded into the surface of the tested scaffolds, three of each group ( $n=3$ ), on a 24-well plate and incubated at 37°C in 5% CO<sub>2</sub> humid atmosphere. At determined time points, the viability of cell cultures that developed over scaffolds' surface was determined by adding 5 mM of resazurin solution (Sigma Aldrich) into each well and incubated at same conditions as before for a period of 2 h to allow the reaction. After incubation, 100 µL of the supernatant (medium with the dye) of each sample was transferred to a 96-well plate in quadruplicate and the fluorescence was determined using a fluorescent plate reader (FLUOstar Omega, BMG Labtech) at wavelengths of 540 nm for excitation and 590 nm for emission. The experiment was performed in triplicate.

#### **3.7.2 Evaluation of oxidative stress**

The ability of scaffolds to reduce or to promote the formation of ROS when in contact to cells was analysed through H<sub>2</sub>-DCFDA, a fluorescent intracellular probe for ROS. To perform this assay,  $2 \times 10^5$  cell/mL were seeded into the surface of scaffolds, three of each group ( $n=3$ ), on a 24-well plate and incubated at 37°C in a humid atmosphere with 5% CO<sub>2</sub> with the medium being change twice a week. After 28 days of incubation, the scaffolds seeded with cells were incubated with 100 µL of H<sub>2</sub>-DCFDA probe for 30 min at 37°C in 5% CO<sub>2</sub> humid atmosphere for the internalization of the probe. After, the excess probe was removed and fresh RPMI 1640 medium was added to each well. Oxidative stress was induced by adding 500 µM of H<sub>2</sub>O<sub>2</sub> to each scaffold and 1 mg/mL of ascorbic acid was added to one of the triplicates of each group to be the control. Fluorescence from each well was measured using a microplate fluorescent reader (FLUOstar Omega, BMG Labtech) at the wavelengths of 485 nm for excitation and 520 nm for emission.

#### **3.7.3 Evaluation of PLA scaffolds osteogenic potential**

To evaluate the capacity of PLA scaffolds to promote the cellular proliferation and differentiation into bone cells (osteogenic capacity), two characteristic elements of bone cells and bone formation were analysed: the activity of the alkaline phosphatase (ALP activity) and the mineralization of the matrix through the Alizarin Red stain method (73) for staining the deposits rich in calcium present in the cells. To perform the assays,  $2 \times 10^5$  cells/mL of MG-63 cells were seeded into the surface of the tested scaffolds, three of each group ( $n=3$ ), on a 24-well plate and

incubated at 37°C in 5% CO<sub>2</sub> humid atmosphere with the medium changed twice a week. At day 28, the assays were conducted. Both experiments were performed in duplicate.

#### **Alkaline Phosphatase activity**

The ALP activity was evaluated using the BCIP-NBT assay (Sigma Fast) and for that scaffolds with the seeded cells, at day 28, were washed twice with a solution of NaCl 0.9% and 700 µL of BCIP-NBT solution, prepared according to the manufacturer's protocol, were added to each scaffold and incubated at 37°C in 5% CO<sub>2</sub> humid atmosphere. After incubation, photos (Leica camera) were taken for the qualitative analysis. Then, 700 µL of 10% SDS-HCL solution was added to the scaffolds, to solubilize the violet crystal, and incubated overnight at 37°C. After, the crystals were solubilized, 100 µL of the supernatant of each sample was transferred in quadruplicate to a 96-well plate and the absorbance was measured using a plate reader (FLUOstar Omega, BMG Labtech) at 495 nm. ALP activity of MG-63 cell was normalized for viable cells.

#### **Alizarin Red stain assay**

The scaffolds with the seeded cells, after 28 days of incubation, were washed 3 times with PBS pH 7.4 10 mM (Sigma-Aldrich) and 3x with water. After the washing step, cell-scaffolds were stained by adding 700 µL of Alizarin Red Stain (GeneCopoeia) solution for 30 min at RT and covered from the light. Cell-scaffolds were subjected to several washing steps with distilled water until the water was translucent and photos (Leica camera) were taken for qualitative analysis. To quantify the calcium deposits on the scaffolds the red precipitate was solubilized by adding 700 µL 5% SDS on 0.5M HCl (AppliChem, GmbH) over night at RT. After solubilization, 100 µL of the supernatant of each sample was transferred in quadruplicated to a 96-well plate and the absorbance was read at 405 nm. A scaffold from each group without seeding cells was used as blank and the Alizarin was normalized for the blanks and for the viable cells.

### **3.8 Magnetic heating properties – Thermal studies**

Magnetic heating properties were evaluated by placing the samples inside an induction coil using an induction heating system, the EasyHeat equipment (Ambrell), and surround the sample with an isolating box, as can be seen in Figure 3.2. The temperature was measured with an optical fiber temperature sensor.

Hyperthermia studies were conducted on physical department at Faculdade de Ciências from Universidade de Lisboa with the kind help of Professor Maria Margarida Cruz and Professor Liliana P. Ferreira.

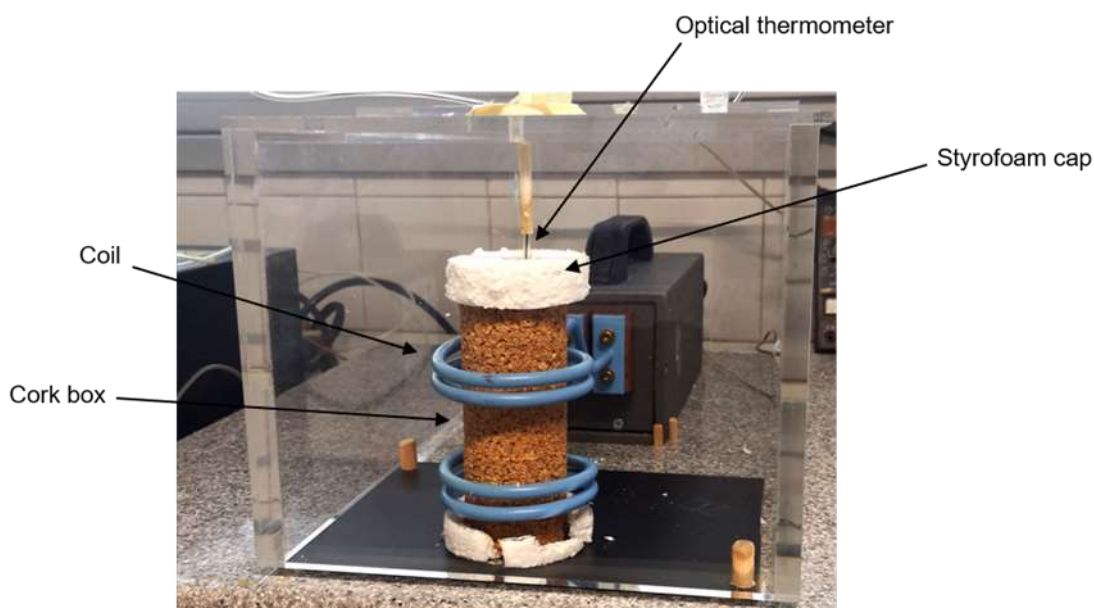


**Figure 3.2** Isolated heating unit for evaluation of heating properties

#### **SPIONs magnetic heating properties**

The magnetic nanoparticles were mixed in distillate water to a concentration of 1 mg/mL, and 1 mL of the solution was in a water bath at 36°C, mimicking the body temperature, before being subjected to an alternating magnetic field (AMF) of 372 A and 275 kHz frequency for 30 min (1800 sec).

#### **Scaffolds magnetic heating properties**

The G5: PLA-Col-nHA-SPIONs-MH was tested for magnetic heating properties and an additional group without SPIONs, namely PLA-Col-nHA-MH was used as control. For that, scaffolds were placed with 1 mL of RPMI 1640 medium and heated in an AMF of 372 A and 275 kHz for around 1 h 20 min (4800 sec).

### **3.9 Statistical analysis**

Statistical analysis was performed using GraphPad Prism version 7.0. Statistical comparison among experimental groups were performed using the one-way ANOVA followed by Tukey's multiple comparisons test and the statistical significance was defined as  $p < 0.05$ . All data were expressed as mean  $\pm$  SD.

# 4.

## 4 Results

### 4.1 SPIONs fundamental characterization

#### 4.1.1 Zeta potential of SPIONs

Zeta Potential measurements revealed that SPIONs in water have a positive surface charge and in the remaining media have a negative surface charge (Table 4.1). Results suggest that the negatively charged molecules present in the PBS solution, the RPMI 1640 medium and the BHI medium will bind to the SPIONs surface modifying their surface charge.

It is also possible to observe that an acidic pH, characteristic of infection sites, will not change the surface charge of the SPIONs when compared to the physiological pH.

**Table 4.1** Zeta potential (mean  $\pm$  SD) of SPIONs measured in different media (n = 3)

Media	Zeta Potential (mV)
H <sub>2</sub> O	+21.1 $\pm$ 0.8
PBS 10 mM pH 7.4	-29.3 $\pm$ 2.4
PBS 10 Mm pH 6.5	-29.2 $\pm$ 1.3
RPMI 1640 medium	-26.4 $\pm$ 1.8
BHI medium with 1% glucose	-30.1 $\pm$ 1.8

#### 4.1.2 *In vitro* evaluation of SPIONs oxidative stress

The potential capacity of SPIONs to induce oxidative stress was evaluated measuring the intracellular ROS production through an intracellular probe which becomes fluorescent in the presence of ROS, therefore the ROS generation is directly proportional to the increase of fluorescent intensity. After MG-63 cells were exposed to different concentrations of SPIONs (1, 0.5 and 0.25 mg/mL) for different periods of time (3, 6 and 24 h), it was observed that with 3 h exposure there is no significant increase in fluorescence intensity in comparison with negative control cells (untreated cells group), as can be seen in Figure 4.1. However, after 6 h of exposure, it is visible a significant increase in fluorescence intensity of the three SPIONs concentrations in comparison with the untreated cells, meaning more ROS production. It is also noticeable that

there are significant differences in ROS percentage (%ROS) between the SPIONs concentrations 1 mg/mL and 0.5 mg/mL (with  $p < 0.05$ ), revealing that a higher concentration has a higher % ROS. After the 24 h incubation, the fluorescence intensity increased further with higher fluorescence in higher concentrations (with  $p < 0.001$ ). These results allow to conclude that SPIONs induces oxidative stress in a time- and concentration-dependent way.

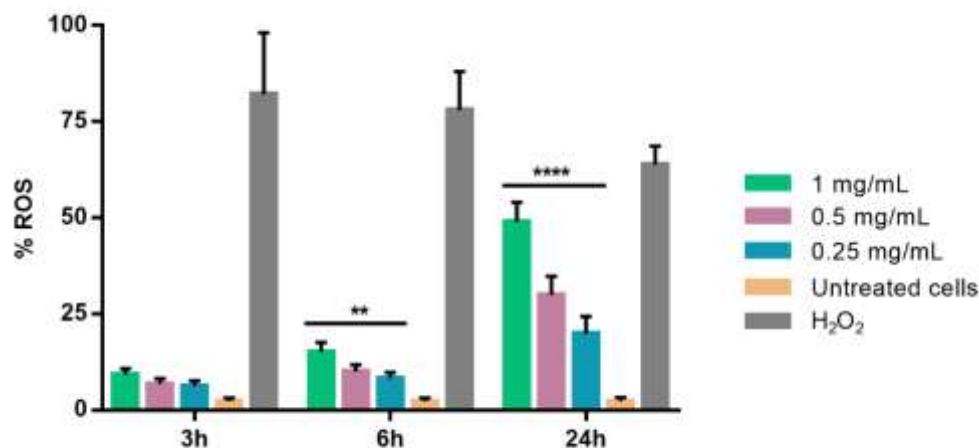


**Figure 4.1** MG-63 cells ROS production when in contact with SPIONs

The percentage of ROS production by MG-63 cells when in contact with different concentrations of SPIONs (1, 0.5 and 0.25 mg/mL) was evaluated for 3, 6 and 24 h periods. A group of untreated cells was used as negative control and a group with H<sub>2</sub>O<sub>2</sub> as positive control. \*\* means that groups below are significantly different with  $p < 0.01$  and \*\*\*\* significantly different with  $p < 0.0001$  from the group of untreated cells.

### 4.1.3 *In vitro* evaluation of SPIONs cytotoxicity

*In vitro* evaluation of SPIONs cytotoxicity was investigated on MG-63 cells, after a period of 24 h of incubation with different concentration of SPIONs, by staining the dead cells with propidium iodide (PI) dye and by identifying the viable ones with AlamarBlue and MTT assays. A group of untreated cells was used as negative control group to compare the data and a group of cells treated with 1 mg/mL of SDS was used as positive control.

The results of the uptake of PI dye, Figure 4.2 (A), showed that the cellular death of the SPIONs groups are significantly lower when compared with the group of untreated cells, meaning less cell death which indicates that SPIONs have no cytotoxicity effect against MG-63 cells at tested concentrations. As well as in the PI assay, the SPIONs in AlamarBlue and MTT assays (Fig. 4.2 (B) and (C), respectively) also demonstrate no cytotoxic effect against MG-63 cells once the cellular viability is close to the 100% viability from the untreated cells group. The 1 mg/mL of SPIONs on AlamarBlue assay (Fig. 4.2 (B)) is significantly different, with  $p < 0.01$ , from the group of untreated cells with an increase of the cellular viability along the decrease of the SPIONs concentration, as expected. Some of the discrepancies observed between the three assays are due to the flaws from the method used because nanoparticles interfere with the fluorescence

reading. Concluding, the three assays agree, which permits to conclude that the SPIONs in the present tested concentrations are biocompatible.

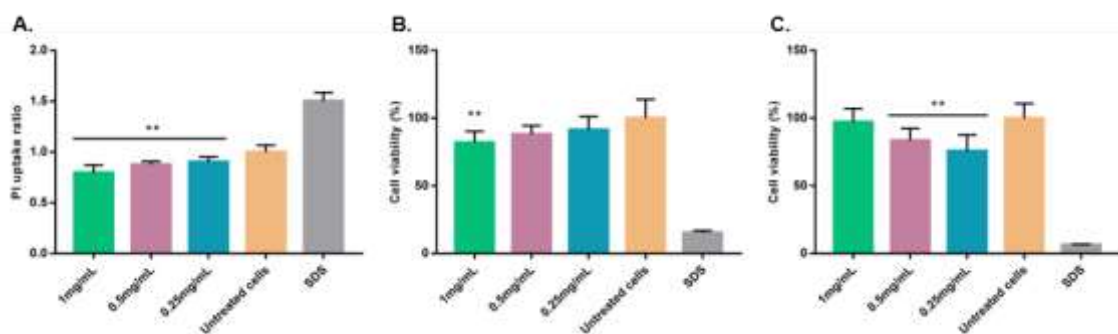


**Figure 4.2** Evaluation of SPIONs cytotoxicity

Evaluation of the effect of different concentrations of SPIONs (1, 0.5 and 0.25 mg/mL) on MG-63 cell proliferation and viability, exposed for a 24 h period, by the Propidium Iodide (PI) (A), AlamarBlue (B) and MTT (C) assays. For the three assays, data are compared relatively to the values of the untreated cells group (that is = 1.0 PI uptake ratio for the PI assay (A) and = 100% cell viability for the AlamarBlue (B) and MTT (C) assays) and a group of cells were treated with SDS to use as positive control; \*\* means that groups below are significantly different from the group of untreated cells with  $p < 0.01$ .

#### 4.1.4 SPIONs cellular uptake study

SPIONs, as a successful candidate for biomedical application, depends on their localization and delivery into cells. Therefore, SPIONs cellular uptake and localization was studied under fluorescence microscopy analysing two different concentrations of SPIONs (C1 - 0.5 mg/mL and C2 - 1 mg/mL) exposed to cells for two periods of time (t1 – 1 h exposure and t2 – 14 h exposure). The control groups were not exposed to SPIONs. The results, presented in Figure 4.3, display SPIONs harshly associated with cells, once in both concentration of both exposure times SPIONs concentrate attached to cell membranes (red arrows). With increased exposure time, it is possible to observe the intracellular presence of nanoparticles inside the nucleus of cells (white arrows), which happens in both concentrations of time t2 (14 h exposure).

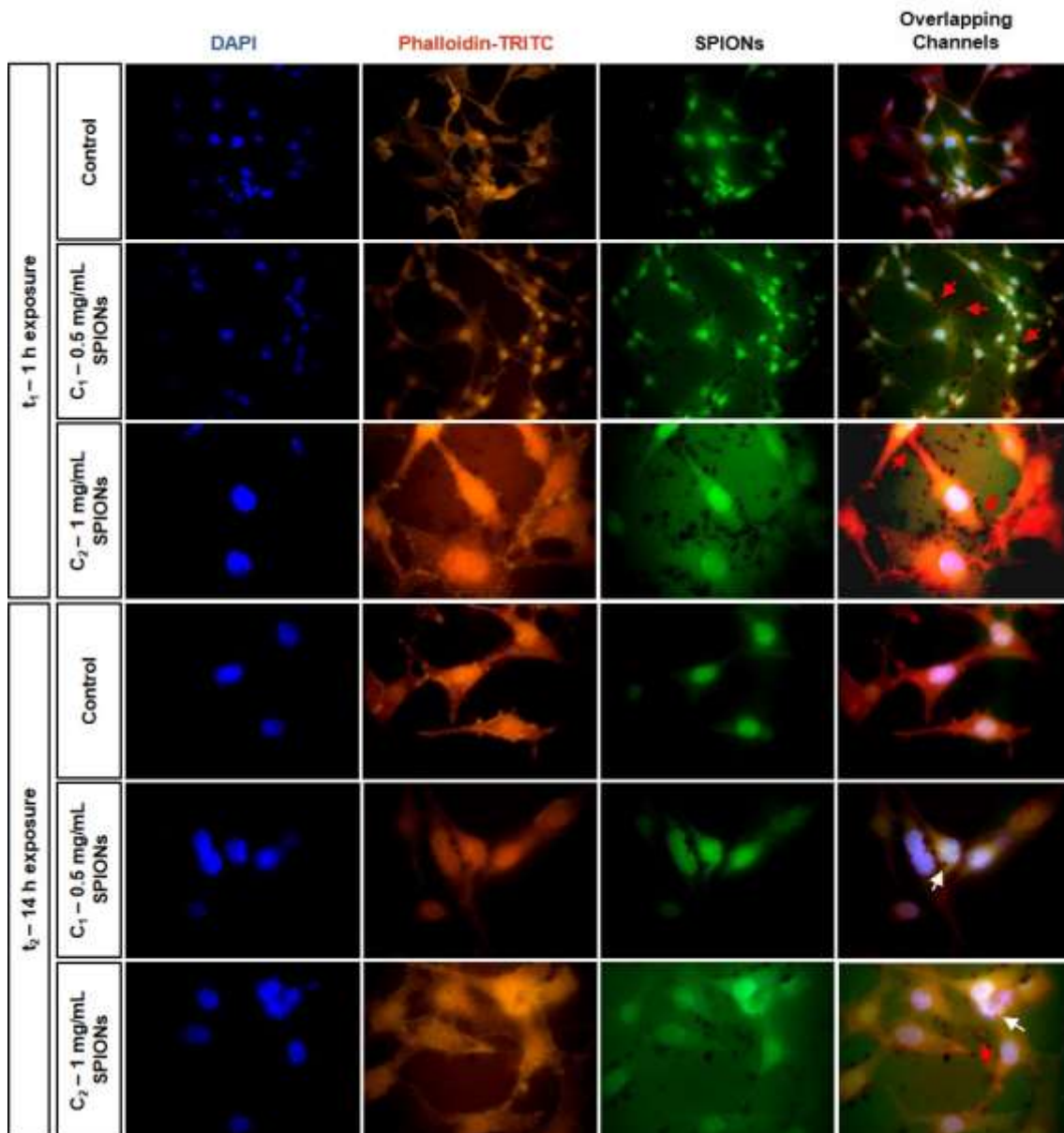


**Figure 4.3** Cellular localization of SPIONs

Fluorescence microscopy images of MG-63 cells exposed to two different SPIONs concentrations, C1 - 0.5 mg/mL and C2 - 1 mg/mL, for two different periods of time,  $t_1 - 1\text{ h}$  and  $t_2 - 14\text{ h}$ . Control groups were not exposed to SPIONs. Nucleus were stained with DAPI (blue), the cytoskeleton with phalloidin-TRITC (orange/red) and the SPIONs (black dots) are visible without staining. The nanoparticles concentrate attached to the cell membranes (red arrows) and, at long time exposure, they are also localized inside the nucleus (white arrows).

## 4.2 Characterization of functionalized PLA scaffolds

### 4.2.1 Morphological and chemical characterization

In this study, 3D printed PLA scaffolds were successfully functionalized with the surface adsorption method, as can be seen through the morphological analysis in Figure 4.4. Photos of functionalized scaffolds (Fig. 4.4 A.1 – A.5) exhibit different coloration according to the corresponding compounds of functionalization, namely G1: PLA-Col remained white, while G2: PLA-Col-nHA changed to a beige colour due to hydroxyapatite, G3: PLA-Col-SPIONs to a

brownish colour characteristic of the iron oxide, G4: PLA-Col-nHA-SPIONs to a dark beige and G5: PLA-Col-nHA-SPIONs-MH changed to a yellowish colour attributed to MH.

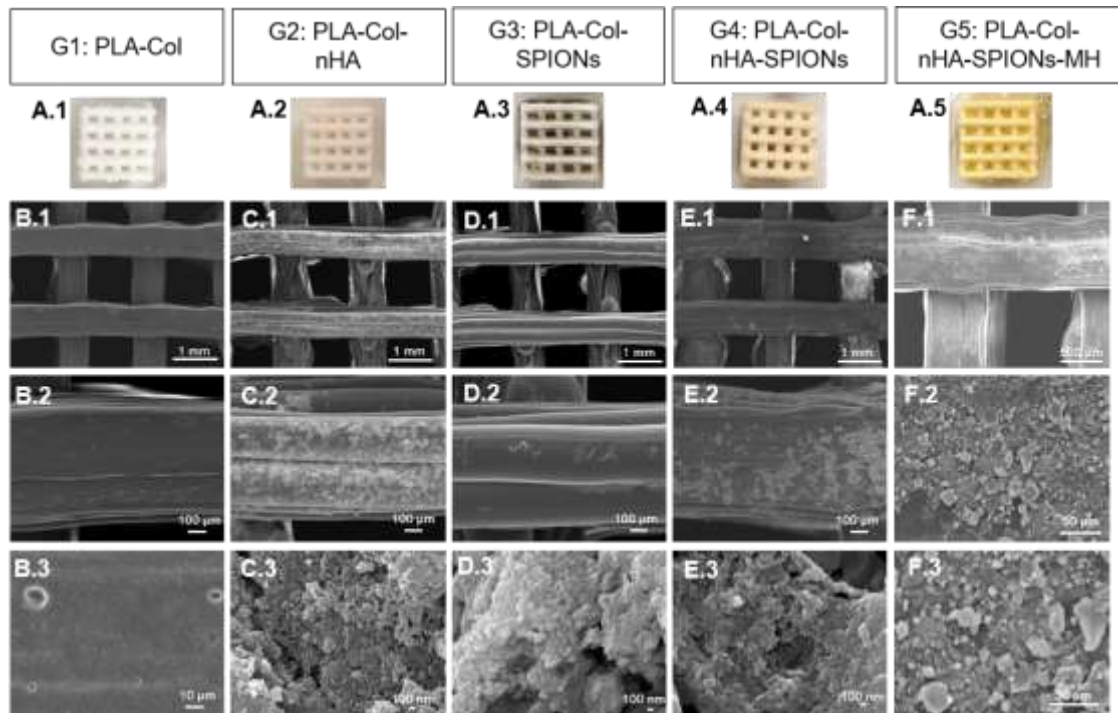


**Figure 4.4** Morphological characterization of functionalized PLA scaffolds

Images of functionalized 3D printed PLA scaffolds (**A.1 – A.5**), evidencing the different coloration between scaffolds according to the surface coating and SEM images, with different magnifications, (**B – F**) where **B.1** to **B.3** correspond to G1: PLA-Col, **C.1 to C.3** to G2: PLA-Col-nHA, **D.1 to D.3** to G3: PLA-Col-SPIONs, **E.1 to E.3** to G4: PLA-Col-nHA-SPIONs and **F.1 to F.3** to G5: PLA-Col-nHA-SPIONs-MH. The different nanoparticles were observed coating the PLA surface by the presence of nHA with a rod-shape (**C**), of SPIONs with a spherical form (**D**) and the presence of both (**E and F**), while (**B**) showed the surface only coated with collagen.

SEM images (Fig. 4.4 B - F) allowed to confirm that 3D printed PLA scaffolds have square pores with around 1000  $\mu\text{m}$  of size and to evaluate the nanoparticles surface adsorption. Comparing the groups 2, 3, 4 and 5 with group 1 it was observed the presence of nanoparticles distributed around all over the scaffolds surface, with clusters of nanoparticles in some areas, confirming that the adsorption method was well achieved in groups coated with nanoparticles. It was also observed that nHA have a rod shape and SPIONs a spherical form, visible in Figure 4.4 C.3 and D.3, respectively. These differentiating features allowed to affirm that both nanoparticles were adsorbed at the surface of PLA of groups 4 and 5, coated with nHA and SPIONs (Fig. 4.4 E.3 and F.3). SEM analysis also allowed to compare the presence and distribution of both nanoparticles on PLA surface, in which can be said that nHA have a better distribution as well a better attachment than SPIONs (Fig. 4.4 C.2 and D.2).

EDS analysis allowed to identify the elemental chemical composition of scaffolds surface, where it was observed the presence of calcium (Ca) and phosphorus (P) ions in G2: PLA-Col-nHA scaffolds (Fig. 4.5 B), and iron (Fe) ions in G3: PLA-Col-SPIONs (Fig. 4.5 C), which results of the coating with nHA and SPIONs, respectively. In G4: PLA-Col-nHA-SPIONs and G5: PLA-Col-nHA-SPIONs-MH, it was observed the presence of the three ions, Ca, P and Fe, conforming

the presence of both nanoparticles in the PLA surface (Fig. 4.5 D and E). None of the ions are present in G1: PLA-Col, as expected (Fig.4.5 A).

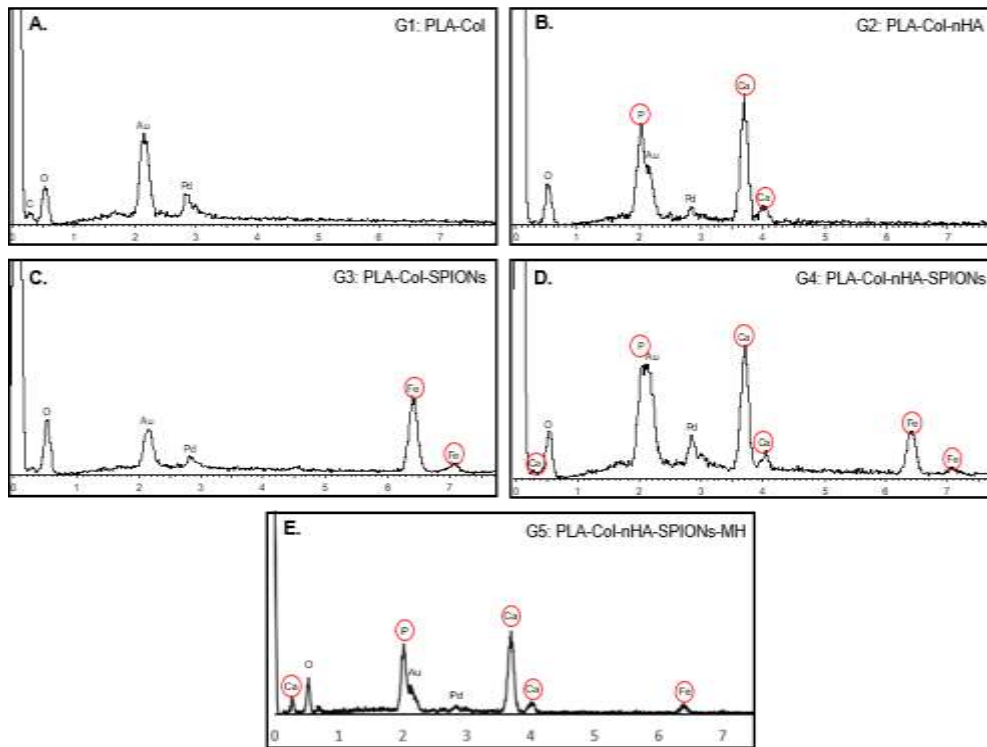


**Figure 4.5** Chemical composition of functionalized PLA scaffolds surface  
EDS analysis of PLA scaffolds of five groups: **A.** G1: PLA-Col, **B.** G2: PLA-Col-nHA, **C.** G3: PLA-Col-SPIONs, **D.** G4: PLA-Col-nHA-SPIONs and **E.** G5: PLA-Col-nHA-SPIONs-MH, showing the presence of nanoparticles on PLA surface through the presence of the corresponding ions. Calcium (Ca) and phosphorus (P) ions in scaffolds adsorbed with nHA (**B.**, **D.** and **E.**) and iron (Fe) ions in scaffolds adsorbed with SPIONs (**C.**, **D.** and **E.**).

SEM images and EDS analysis allowed to prove that nHA and SPIONs were successfully incorporated into PLA surface by the adsorption method used, concluding that this coating method is efficient and stable.

#### 4.2.2 Swelling behaviour

In the present study, the *in vitro* water absorption was measured to evaluate the swelling ability of the five groups of PLA scaffolds in study plus two additional groups, namely PLA without alkali hydrolysis treatment (AHT) and PLA with AHT, with the aim of analyse the influence of AHT in the swelling ability of the scaffolds. The swelling behaviour of PLA scaffolds is shown in Figure 4.6., where are only represented the three scaffolds groups with the biggest difference between their swelling ability: PLA with AHT, PLA-Col and PLA-Col-nHA-SPIONs-MH. The graphics of the remaining groups are in Appendix A.

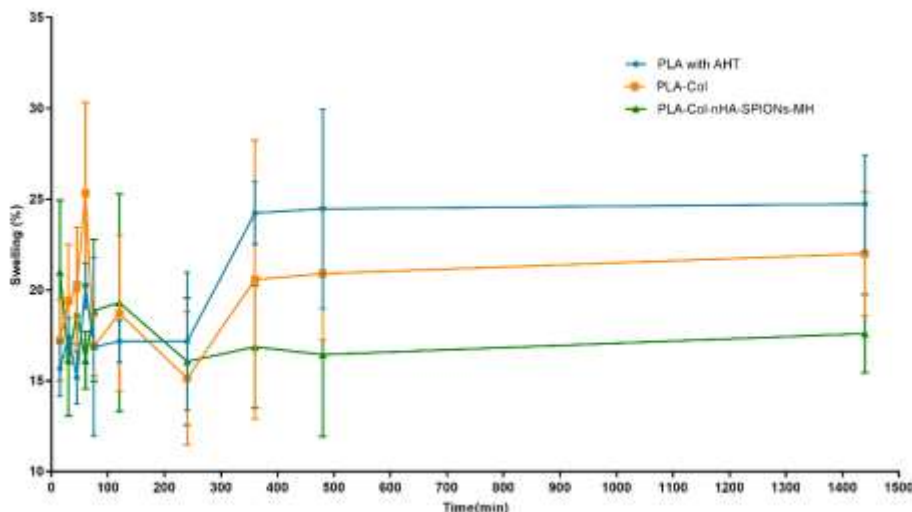


**Figure 4.6** Swelling ability of PLA scaffolds from G1, G5 and PLA with AHT

Graphic representation of the *in vitro* swelling behaviour, in percentage, of PLA scaffolds (n=3) groups with the biggest differences, measured for a period of 24 h (1440 min), where it is possible to observe a low swelling ability of the groups here represented with a maximum swelling capacity of 24.7% of the group PLA with AHT (in blue).

The characterization of PLA scaffolds swelling behaviour revealed, in general, a low capacity to absorb water and, through the graphic observation (Fig. 4.6 and Fig. A1), it is possible to verify that all groups in study have a similar swelling ability, with the absorption increase at the first hour, followed by a period of inconstant swelling ratio, with multiple variation in the swelling ratio, and then reaching a constant rate at 8 hours (480 min). The group PLA with AHT has a higher swelling ability than PLA without AHT, with a swelling capacity, at 24 h, around 24.7% and 17.7%, respectively. This proves that the alkali hydrolysis treatment achieves its purpose of increase PLA hydrophilicity. When adsorbing compounds, Col, SPIONs, MH and mainly nHA (67) to PLA surface, the capacity to retain water decreases, as expected, with G1: PLA-Col, G2: PLA-Col-nHA, G3: PLA-Col-SPIONs, G4: PLA-Col-nHA-SPIONs and G5: PLA-Col-nHA-SPIONs-MH having, at 24 h, a swelling capacity of 22%, 15%, 16.9%, 22.7% and 17.6%, respectively.

### 4.2.3 *In vitro* minocycline release study

Aiming the investigation of antibiotic MH release performance, the release profile of PLA scaffolds from G5: PLA-Col-nHA-SPIONs-MH was investigated, at pH 7.4, and the results are showed in Figure 4.7. It is possible to observe that MH was released, meaning that the antibiotic was efficiently adsorbed into the scaffold by the method used. Release profile of the drug shows a burst release within the first 15 min, becoming slowly released after 2 h (120 min), occurring discharge to the medium until 28 h (1680 min) of the assay.

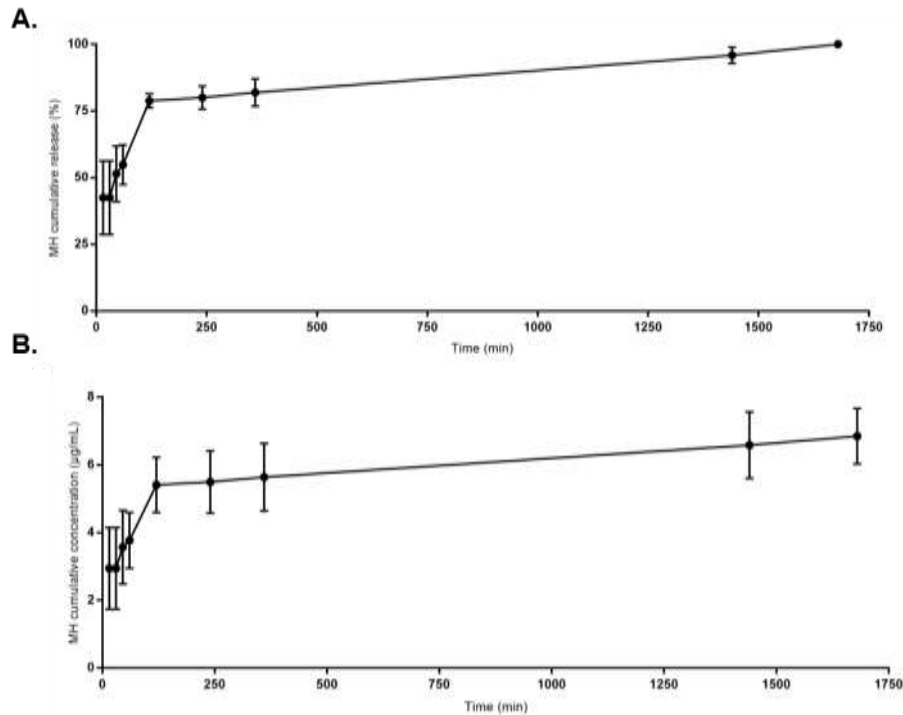


**Figure 4.7** *In vitro* release profile of MH from PLA scaffolds

Release profile of PLA scaffold loaded with antibiotic minocycline (G5: PLA-Col-nHA-SPIONs-MH) during a 28 h (1680 min) period, where **A.** is the cumulative release in percentage and **B.** the cumulative release in concentration ( $\mu\text{g/mL}$ ) of the antibiotic minocycline ( $n=3$ ).

In the first 15 minutes of release, PLA scaffolds had released  $42.5 \pm 13.8\%$  of the antibiotic corresponding to  $2.9 \pm 1.2 \mu\text{g/mL}$ , raising the possibility of a non-cytotoxic effect when tested in cells, and the 100% minocycline discharge was achieved at 28 h (1680 min), reaching  $6.8 \pm 0.8 \mu\text{g/mL}$  of antibiotic. These results also suggest that, although there was MH adsorption into the scaffold, and presupposing that it releases everything that adsorbs once PLA scaffolds lost their yellowish colour (characteristic from MH presence), it was only a small amount of MH that was adsorbed, around 1.36% of the initial concentration of minocycline ( $500 \mu\text{g/mL}$ ).

#### 4.2.4 *In vitro* bioactivity study

An orthopaedic material with bone regeneration purpose need to be bioactive and capable of improve the interface between the material and the bone tissue, because of that *in vitro* biomineralization of scaffolds was carried out by immersion in SBF solution and RPMI 1640 medium at  $37^\circ\text{C}$  for a 4 weeks period and analysed through ATR-FTIR spectroscopy, SEM imaging and EDS maps. The ATR-FTIR spectra of G5: PLA-Col-nHA-SPIONs-MH after soaking in SBF is shown in Figure 4.8 A. where it is possible to observe the emergence of the  $\text{PO}_4$  characteristic absorption band in the range of  $1040\text{-}1090 \text{ cm}^{-1}$  and a broad band at  $3503 \text{ cm}^{-1}$  corresponding to the -OH group right after 1 week soaking in SBF. Both  $\text{PO}_4$  and -OH are chemical functional groups characteristics from HA that forms the apatite layer (74,75). Looking at the spectrum it is also observed that there seems to be a cycle of mineralization and dissolution of HA characteristic groups over the weeks.

The morphology of G5 scaffolds after 1 week and 2 weeks immersion is shown in Fig. 4.8 B.1 and C.1, respectively. In SEM images of the scaffold after 1 week immersion, it is observed shining protuberances on the scaffold's surface, that corresponds to bone-like apatite regions, increasing to a bone-like apatite sheet in week 2 that covers the surface, assuming that over time the apatite layer increases. The mineralization on the scaffolds surface is confirmed by EDS maps of Ca and P (Fig. 4.8 B.2 – 3 and C..2 – 3). ATR-FTIR and SEM images are in agreement, exhibiting the deposition of a bone-like apatite layer which, evidences the scaffolds bioactivity.

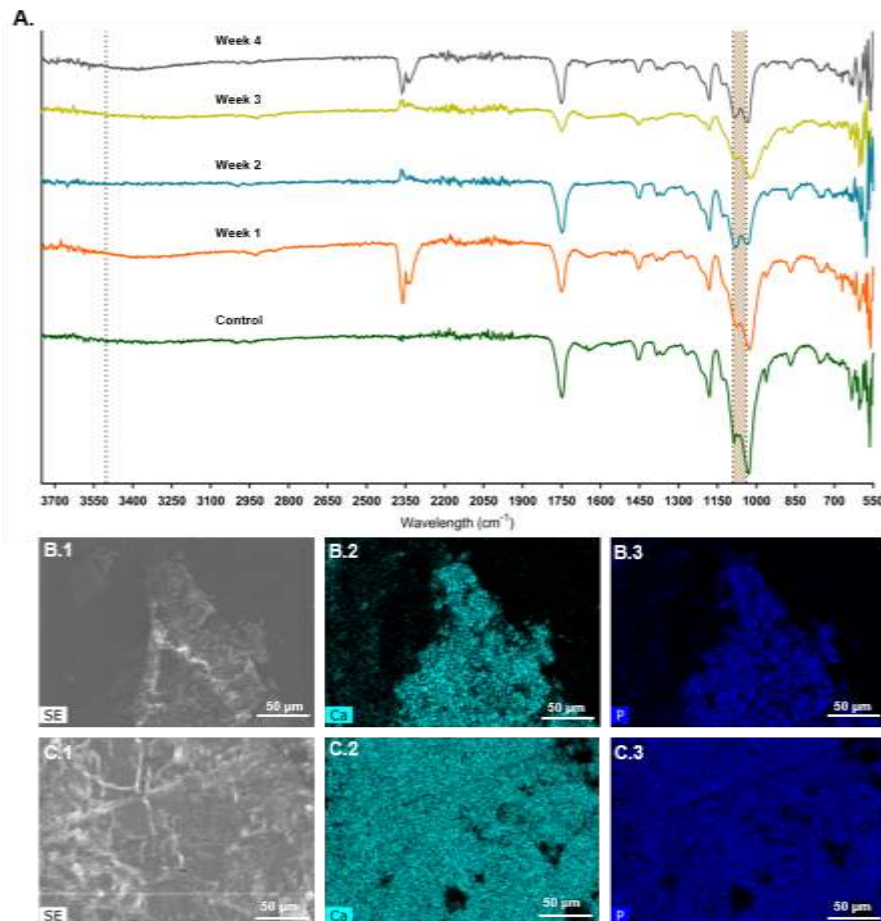


**Figure 4.8** Bioactivity of G5: PLA-Col-nHA-SPIONs-MH in SBF solution

Bioactivity evaluation of scaffolds from G5: PLA-Col-nHA-SPIONs-MH immersed in SBF for 4 weeks through ATR -FTIR spectra in (A) with the band characteristic of  $PO_4$  groups ( $1040-1090\text{ cm}^{-1}$ ). (B) and (C) are SEM images in (1) and EDS maps of Ca in (2) and P in (3) after 1 week and 2 weeks of immersion in SBF, respectively, where it is possible to observe the formation of an apatite-layer by the shining protuberances in SEM images.

ATR-FTIR spectra of the remaining groups of scaffolds immersed in SBF and the scaffolds immersed in RPMI 1640 culture medium, that better mimics the body environment with the presence of amino acids, proteins, nutrients and others, are shown in Appendix B. Observing all the spectra (Fig. 4.8 and Fig. B1 - B3), the presence of nHA is responsible for the changing in bands characteristic of the chemical groups of HA, that forms the apatite layer, meaning that nHA is favouring the scaffolds bioactivity. Between SBF solution and RPMI 1640 medium, spectra have slight differences possibly due to their different composition. pH changes of SBF solution

and RPMI 1640 culture medium over weeks are also given in the Appendix B, where it is possible to observe a raise in the pH in the first week of immersion.

### 4.3 Microbiological studies: evaluation of antimicrobial activity

#### 4.3.1 Agar diffusion and biofilm inhibition assays

The agar diffusion test (Figure 4.9) showed that G5: PLA-Col-nHA-SPIONs-MH inhibited bacterial growth, with an inhibition zone measuring  $27.7 \pm 2.2$  mm of diameter (Fig.4.9 C.), which is in accordance with the value that resulted from the positive antibiotic controls (30  $\mu$ g of MH), that exhibit an average diameter of  $29.3 \pm 1.0$  mm (Fig. 4.9 D.). Both measured diameters are between the expected values for the diameter produced by MH in *S. aureus* ATCC 25923 (between 25 and 30 mm), according to the values stipulated by CLSI (76), validating this assay and allowing to state that G5: PLA-Col-nHA-SPIONs-MH have an effective antibacterial effect. No inhibition zone was observed in the remain studied samples (G2: PLA-Col-nHA and G4: PLA-Col-nHA-SPIONs), as happens in negative control (distilled water) (Fig.4.9 A., B. and E.).

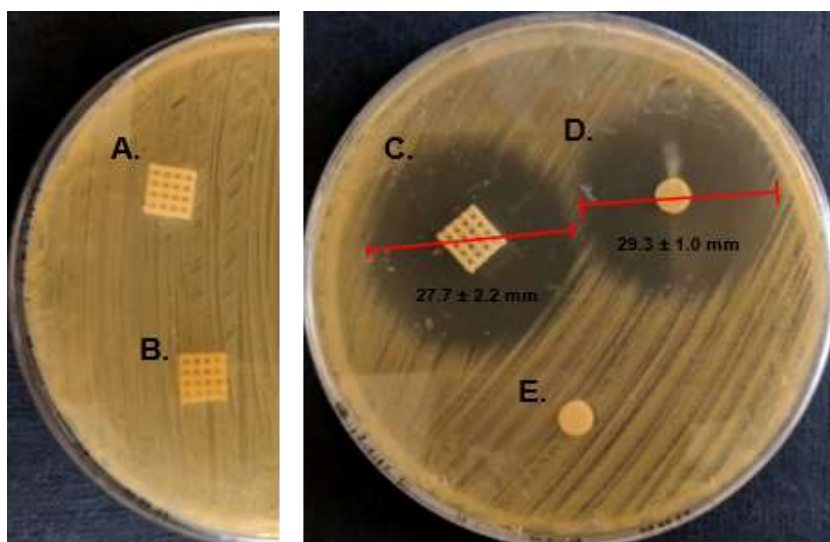


**Figure 4.9** Agar diffusion assay against *S. aureus*

Optical images of the evaluation of the antimicrobial activity against *S. aureus* (ATCC 25923) by the agar diffusion assay: **A.** G2: PLA-Col-nHA, **B.** G4: PLA-Col-nHA-SPIONs, **C.** G5: PLA-Col-nHA-SPIONs-MH, with) as **D.** positive control, MH (30  $\mu$ g) and **E.** negative control (distilled water).

The evaluation of PLA scaffolds activity against *S. aureus* biofilm formation was performed by SEM analysis, showed in Figure 4.10. It is observed a biofilm of *S. aureus* completely covering the scaffolds surface of G2: PLA-Col-nHA and G4: PLA-Col-nHA-SPIONs (Fig. 4.10 A. and B., respectively). On the contrary, it is not observed biofilm formation (Fig. 4.10 C.) on the surface of scaffolds from the group loaded with the antibiotic minocycline (G5: PLA-Col-nHA-SPIONs-MH). These both tests come state that G5: PLA-Col-nHA-SPIONs-MH have an antimicrobial effect and an antibiofilm formation against *S. aureus*. Contrary to what was expected, the group in study

with the SPIONs (G4: PLA-Col-nHA-SPIONs), showed a higher formation of biofilm compared with the group without SPIONs (Fig. 4.10 A. and B., respectively).

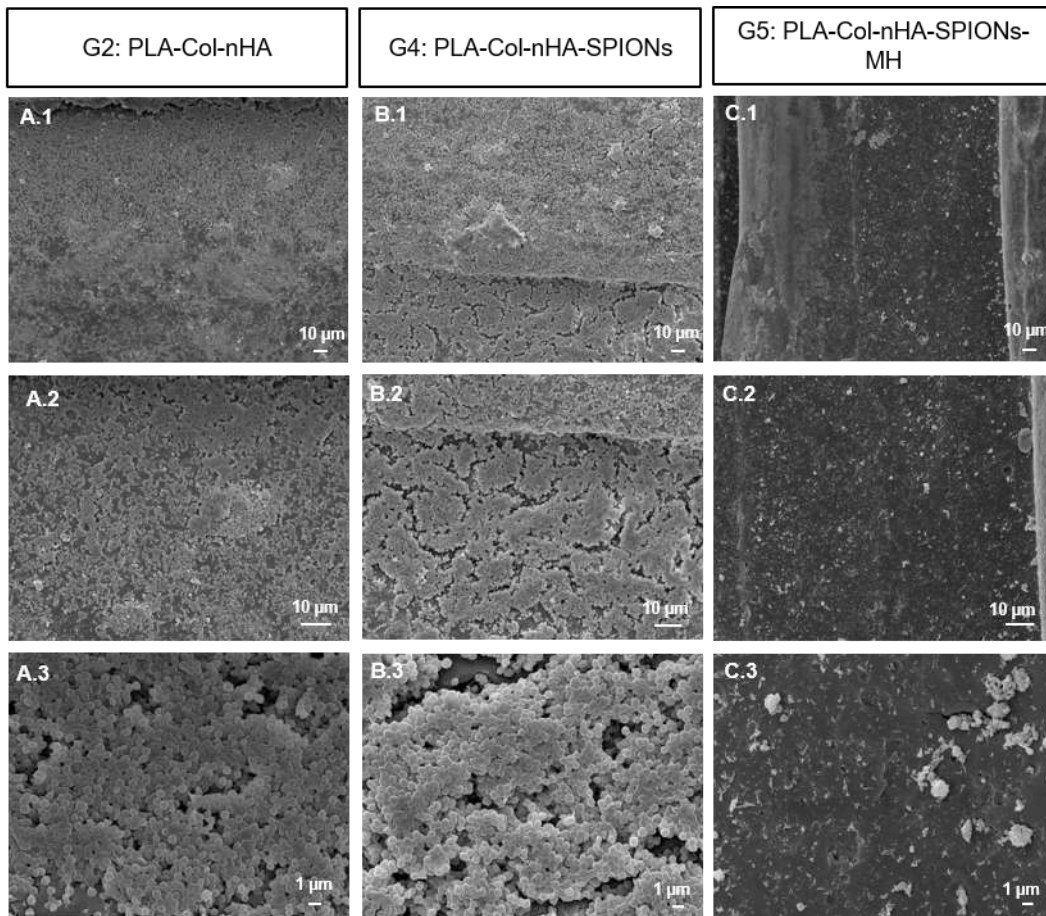


**Figure 4.10** Assessment of biofilm formation on PLA scaffolds surface

SEM images with different magnifications of the evaluation of the antibiofilm properties against *S. aureus* (ATCC 25923) of **A.** G2: PLA-Col-nHA, **B.** G4: PLA-Col-nHA-SPIONs and **C.** G5: PLA-Col-nHA-SPIONs-MH, showing the formation of biofilm at **A.** and **B.**, with the presence of numerous colonies on the scaffolds surface, and showing the inhibition of biofilm formation at the group loaded with the antibiotic minocycline at **C.**

G1: PLA-Col and G3: PLA-Col-SPIONs were not tested for these assays once it is already known that PLA and Col do not have an antibacterial effect.

#### 4.4 *In vitro* cellular studies

##### 4.4.1 Cytocompatibility and cell proliferation

One of the principal requirements of materials for bone tissue applications is their biocompatibility and capability to support cellular growth and proliferation, for that cytocompatibility and cell proliferation of functionalized PLA scaffolds were assessed. PLA scaffolds of each group were incubated, for a period of 28 days, with MG-63 cells and the proliferation was determined by AlamarBlue assay for 14 (week 2), 21 (week 3) and 28 days (week 4) of culture with the aim of assessing the biocompatibility. MG-63 cells seeded on scaffolds

showed to actively proliferate over the surface of all the tested groups, as can be seen in Figure 4.11. No significant difference was observed among the five scaffolds groups in the study, exhibiting values of cell viability equal to the control group (G1: PLA-Col), except for G5: PLA-Col-nHA-SPIONs-MH at day 14 (week 2), which is significantly different from the remaining groups due to the initial burst release of MH, but which cell proliferation recover over time being around the same values of the control group soon in week 3. None of the 5 groups of scaffolds revealed cytotoxic for MG-63 cells.

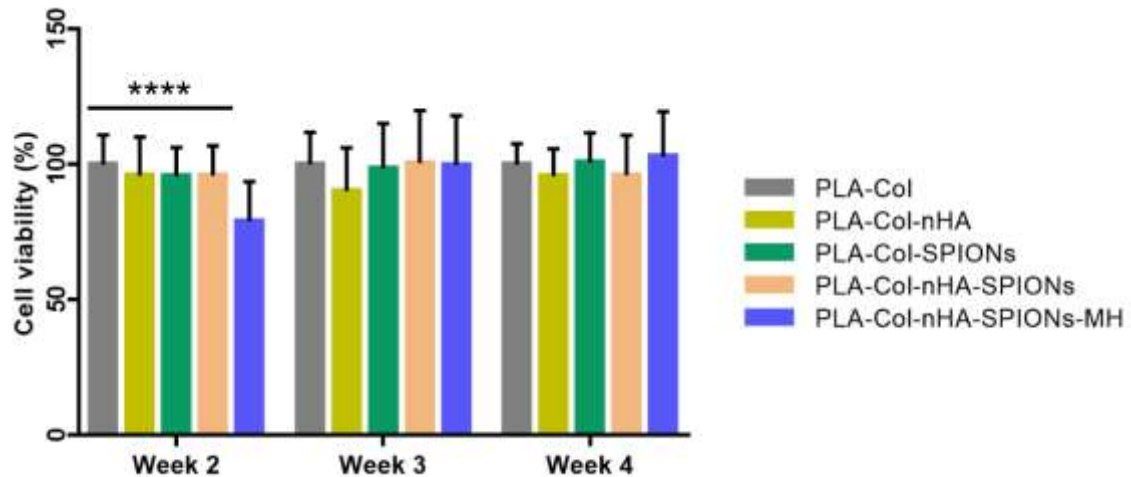


**Figure 4.11** PLA scaffolds *in vitro* cytocompatibility

Cell viability evaluation by AlamarBlue assay after 28 days of MG-63 cells cultured with PLA scaffolds (n=9), where \*\*\*\* are significantly different from PLA-Col-nHA-SPIONs-MH with  $p < 0.0001$ . (mean  $\pm$  SD).

#### 4.4.2 Evaluation of oxidative stress

The potential capacity of PLA scaffolds, especially the PLA scaffolds with SPIONs (8) to induce oxidative stress was evaluated measuring the intracellular ROS production through an intracellular probe which becomes fluorescent in the presence of ROS, as used earlier in the present study. After MG-63 cells have been incubated with the 5 groups of PLA scaffolds, for a 28 days period, and the probe has been internalized, the oxidative stress was induced adding  $H_2O_2$ . ROS percentage (%) of PLA scaffolds, observed in Figure 4.12, is only due to the added  $H_2O_2$  being no significant difference between the five groups of scaffolds tested. PLA scaffolds do not promote ROS production, neither the PLA scaffolds adsorbed with SPIONs. Also, they do not have a protective effect against oxidative stress, once functionalized PLA scaffolds are unable of diminishing the ROS caused by the addition of  $H_2O_2$ , contrary to what is visible for ascorbic acid, a known antioxidant molecule.

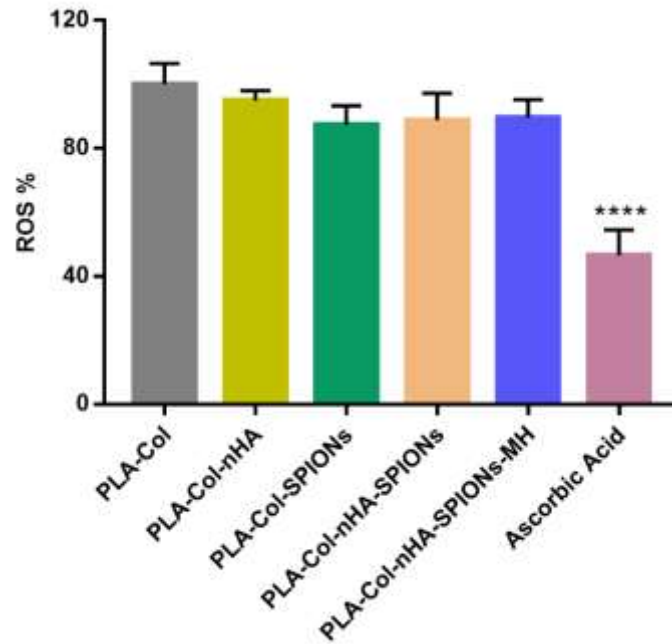


**Figure 4.12** MG-63 cells ROS production when in contact with PLA scaffolds  
Evaluation of ROS production by MG-63 cells when incubated with PLA scaffolds in study for a 28 days period. H<sub>2</sub>O<sub>2</sub> was added to scaffold to induce oxidative stress. A scaffold of each group was treated with ascorbic acid as negative control. \*\*\*\* means significantly different with  $p < 0.0001$  from the remaining groups.

#### 4.4.3 Evaluation of PLA scaffolds osteogenic potential

The ability of PLA scaffolds to promote bone formation was evaluated through ALP activity and Alizarin Red assays, after 28 days of incubation with MG-63 cells, and the results are showed in Figure 4.13. ALP activity, normalized to cellular viability, showed no relevant difference among the groups in study, as can be seen in Figure 4.13 A.2, meaning that any of the compounds adsorbed on the scaffolds surface promoted osteoblastic activity. On the other hand, ECM mineralization of MG-63 cells on PLA scaffolds determined by the Alizarin Red assay normalized to cellular viability, showed on Figure 4.13 B., revealed the formation of more calcium deposits (stained in red) in scaffolds adsorbed with nHA, suggesting that the presence of nHA promote the ECM mineralization. nHA seems to enhance osteogenic capacity of scaffolds, unlike the other compounds that do not improve bone formation.

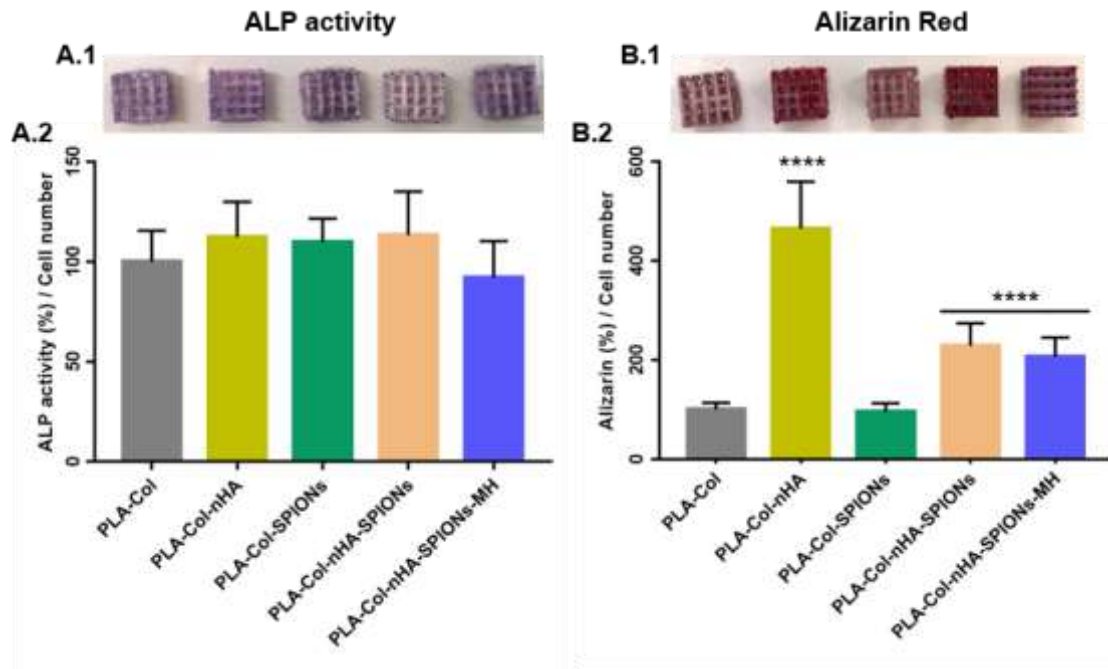


**Figure 4.13** Osteogenic capacity of PLA scaffolds

Evaluation of PLA scaffolds osteogenic capacity, after 28 days of incubation with MG-63 cells, by ALP activity (A.) and Alizarin Red (B.) assays (n=6). A.1 and B.1 are photos of scaffolds showing the qualitative results corresponding to each bar of the graphic below and A.2 and B.2 are the graphical representation of the qualitative results of the assays. In B.2, \*\*\*\* significantly different from the remaining groups with  $p < 0.0001$ . (mean  $\pm$  SD). ALP activity has no differences between the five groups, but the Alizarin red assay show that nHA seems to enhance osteogenic capacity of scaffolds.

#### 4.5 Magnetic heating properties – Thermal studies

The ability of SPIONs to increase the temperature to hyperthermia values (40°C – 45°C) was evaluated measuring the changes in temperature of the surrounding environment, of SPIONs in water and adsorbed at the surface of PLA scaffolds in culture medium, when applied an alternating magnetic field of 372 A strength and 275 kHz of frequency, as seen in Figure 4.14. The temperature of the solution of water and SPIONs increased very slowly (Fig. 4.14 A.), from 35.5°C to 42.5°C, increasing 7°C within 30 min (1800 sec), corresponding to a temperature increase of 0.23°C/min, which not match the ideal temperature rise rate per unit of time for this type of application. In the scaffolds evaluation, the temperature curve of G5: PLA-Col-nHA-SPIONs-MH (Fig. 4.14 B.) showed an extremely slow temperature increase from 20.5°C to 29.5°C within 1 h 20 min (4800 sec) being the curve equal to the curve of the control scaffold without SPIONs (PLA-Col-nHA-MH), meaning that the temperature raise is due to the coils overheating and not due to the presence of SPIONs.

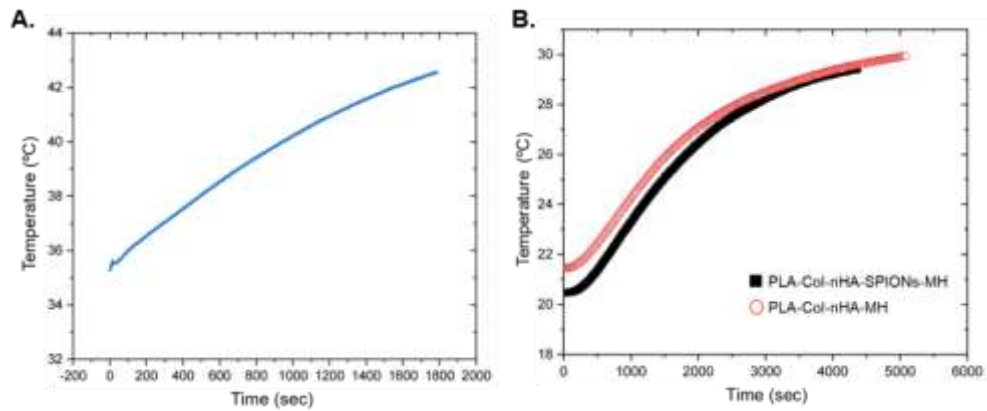


**Figure 4.14** Magnetic heating properties

Temperature curves showing the change in the solutions temperature when applied a magnetic field (magnetic strength of 372 A and 275 kHz of frequency) in the presence of **A.** SPIONs on water and **B.** PLA-Col-nHA-SPIONs-MH (in red) and PLA-Col-nHA-MH (in black), as negative control, on RPMI 1640 medium. SPIONs in water induce an increase of 7°C in 30 min, not corresponding to the ideal time for temperature increase, and both PLA scaffolds in culture medium showed heating of the medium what evidence that the reason is not the presence of SPIONs but are due to the overheating of the coils.



# 5.

## 5 Discussion

The aim of the present study was to develop a novel 3D printed PLA scaffold functionalized with different compounds, with clinically important functionalities, to overcome the difficulties of the actual clinical treatment for bone cancer. One of that compounds was SPIONs for hyperthermia purposes, that by themselves were characterized and *in vitro* cellular studies were performed to conclude about their cytotoxicity and cellular localization. It is known that SPIONs induce cytotoxicity in cancer cells by the production of ROS and the results of the present study showed that occurred ROS production induced by the presence of SPIONs in MG-63 cells, a cell line derived from an human osteosarcoma, in a time and concentration dependent way with 1 mg/mL at 24 h causing the highest ROS production (Fig. 4.1). However, this ROS production seems to be not enough to cause the disruption of the redox homeostasis of cancer cells (37), once cytotoxic assays revealed no cellular death (Fig. 4.2) for the three SPIONs concentrations in study, meaning that SPIONs at those concentration are not cytotoxic. In the cellular uptake study, it is visible that SPIONs are strongly attached to cell membranes after 1 h of incubation (Fig. 4.3). Even more, after 14 h of incubation the SPIONs uptake has increased with internalization occurring (Fig. 4.3), revealing a strong connection to cells that suggests that the cell death could be induced by the magnetic hyperthermia. Even more, it is known that magnetic field potency the SPIONs internalization (37), expecting more SPIONs internalization and a cancer cell death more effective.

After characterizing SPIONs and analyse their cytotoxicity and cellular localization, PLA scaffolds for bone tissue engineering were successfully prepared by a 3D printing technique, submitted to alkaline hydrolysis treatment and functionalized with different combinations of Col, nHA to increase osteoinductivity and osteoconductivity, SPIONs to hyperthermia purposes and MH to avoid infection associated with the scaffold implementation. The 3D printing technique allowed to control the scaffolds morphology and pore size resulting in a regular and uniform macroporous structure with square pores with a size close to 1000  $\mu\text{m}$  (Fig. 4.4), which are aligned with described ideal pore size (20 – 1500  $\mu\text{m}$ ) for bone tissue regeneration, which will favour osteogenesis by allowing vascularization and cell migration promoting bone tissue ingrowth, as well as will support a sustained and efficient drug release required for the release of the antibiotic MH (6,9,16,29), making these scaffolds potential for use in bone tissue engineering applications. The functionalization of PLA scaffolds was successfully achieved by the adsorption method, with the four compounds (Col, nHA, SPIONs and MH) being stably bonded in the PLA

surface as can be verified visually, by SEM images and through EDS analysis in Figures 4.4 and 4.5. It is known that SPIONs are chemically unstable and aggregate easily in solution (37), associating them with PLA scaffolds helped to stabilize them as can be seen in Fig. 4.4, once they stay associated at PLA surface, overcoming one of the obstacles of the usage of SPIONs in the biomedical field.

After achieving an ideal scaffold architecture that promote bone cells growth and that keeps the compounds linked at the surface, the swelling ability of the scaffolds and the release of MH was studied. The swelling ability is the capacity of the scaffolds to absorb and retain fluids and it is an important feature for the bone repair process because excessive fluid absorption modifies the morphology of the scaffold, being a lower swelling ability preferred for bone tissue engineering (69,76). In a general way, all tested groups exhibited a low swelling ratio with values below 25% (Fig. 4.6 and Fig. A1 in Appendix A), suggesting that scaffolds will not suffer any transformation due to the absorption of water and, at the same time, will be able to promote new bone tissue formation. Local antibiotic delivery brings a promising advantage for scaffolds to be applied in bone regeneration, once it prevents more efficiently the growth of bacteria and the formation of biofilm that may come from the surgical intervention (7). In this study, scaffolds loaded with the antibiotic minocycline, that already showed antibiofilm properties in other studies (25), revealed a release profile behaviour of two stages: an initial burst release followed by a progressively slow release (Fig. 4.7). The initial burst release possible resulted from the MH adsorbed on the high surface area of the outer region of the scaffolds and can be advantageous in terms of antimicrobial activity to face the elevated risk of infection that arises soon after the surgical intervention, and the slower release result from the MH present inside the porous structure and may be advantageous by increase bone formation inducing osteoblastic activation and enhancing differentiation into bone cells, important in early stages of bone regeneration (9,25,55,77). The results indicate that the PLA scaffolds could local deliver the antibiotic, being space controlled, in an effective and expected way, however this local release is not totally temporal controlled. Notwithstanding, in studies with similar systems with SPIONs and loaded with drugs, as in Izadi A. et al. (37), it was seen that applying a magnetic field altered significantly the drug release pattern compared to the release pattern without magnetic field, which indicates that the magnetic field triggered the drug release. This suggests that, the scaffolds loaded with MH in the present study, may also respond to the magnetic trigger, enable a more temporal control of MH release from the scaffold.

The results of the release profile of the antibiotic suggest the ability of scaffolds loaded with MH to prevent the bacterial growth and, as the antibiotic is immobilized in scaffolds' surface, to inhibit effectively the biofilm formation. Also, it is known that some SPIONs have antimicrobial activity capable of prevent biofilm formation (56,58). The assessment of antimicrobial activity of scaffolds with MH and SPIONs against *S. aureus* ATCC 25923, a strain that is a strong biofilm producer (25), revealed high antimicrobial and antibiofilm properties of the scaffolds loaded with the antibiotic MH (Fig. 4.9 and 4.10), suggesting that the simple method used to functionalize the scaffolds, composed by a step of adsorption by immersion followed by a step of drying, did not

interfere with MH activity, as well as the remaining compounds of functionalization. Once during the microbiological tests, the optimum conditions for the bacteria proliferation were supplied which results in the maximum bacteria growth in laboratory, it is expected a higher antimicrobial activity in real cases (7), what assures that scaffolds group loaded with MH will play a reliable role in preventing infection. For SPIONs, and in contrary to what was verified by other authors (56), it was observed that the presence of SPIONs in the scaffolds not only does not have the expected antimicrobial effect against *S. aureus*, but also induced greater biofilm growth. The missing antimicrobial effect could be explained by the low concentration of the SPIONs, once the adsorption concentration is 1 mg/mL, but it is not fully adsorbed into the PLA scaffold by the adsorption method used, and for the antimicrobial effect is needed a higher SPIONs concentration. Another possible explanation could be related to the zeta potential of the *S. aureus* bacteria, which is -30 mV (78), and the zeta potential of the SPIONs when they are on the bacteria BHI culture medium, which is  $-30.1 \pm 1.8$  mV. Once both, bacteria and SPIONs, have negative surface charge, they initially repel each other and for the antimicrobial effect, at low SPIONs concentrations, it is needed SPIONs to be attached to the bacteria (58), this is because the key toxicity mechanism by which SPIONs kill bacteria is through the release of free iron ions, next to bacteria, which catalyses the production of reactive oxygen species (ROS), outside the bacteria, inside the bacteria or at the cell membrane, which leads to the oxidative stress with membrane lipid peroxidation, protein oxidation and DNA damage (58). Once SPIONs and bacteria, in this case, initially repel each other and the SPIONs concentration is low, the ROS production will not be effective to kill bacteria, instead the free iron which is released from the SPIONs will act as an exogenous iron source for bacteria, promoting in a second step the growth of bacteria (58), which explains the higher biofilm growth in the presence of SPIONs. Concluding about this SPIONs feature at low concentrations and to maintain the goal of the dual-delivery as part of the bone cancer treatment, becomes even more important to have a local delivery of antibiotic that can be successfully achieved by the MH loading in the scaffolds.

A bioactive material is a material capable of improve the bond between the artificial material and the living bone by promoting the deposition of CaP and HA crystals on its surface (mineralization) that forms a bone-like apatite layer that will encouraging bone cells adherence, bone formation and decreases the possibility of forming a fibrous tissue capsule around the implanted material. So, it is known that a higher bioactivity enhance the cytocompatibility of scaffolds and provides a superior microenvironment for the cell proliferation and bone tissue formation (33,65,76). In the present study, the developed scaffolds proved to be bioactive *in vitro* on SBF solution, especially the scaffolds loaded with nHA, as was already shown by other authors that also correlate the *in vitro* apatite formation on HA with the *in vivo* bond of it to living bone through the apatite layer (65). The presence of  $\text{PO}_4$  and -OH groups characteristic of HA ( $\text{Ca}_{10}(\text{PO}_4)_6(\text{OH})_2$ ) (75), evidenced by changes in the bands corresponding to these groups in the ATR-FTIR spectrum, leads to conclude that is occurring the formation and deposition of hydroxyapatite layers on scaffolds surface, that is visible by the presence of shiny perturbances and sheets over scaffolds surface in SEM images (Fig. 4.8). The increased pH of SBF solution,

when the apatite layer forms, seen by other author as in Farzin A. et al. and Zhao Y. et al. (15,76), is also observed in the present study, stating the bone-like apatite layer formation. The pH increase can be explained by some of the ions present in the scaffolds surface exchange with the  $H^+$  present in the SBF solution, which forms -OH groups on the scaffolds surface and the increase in the pH of SBF (15,76). So, it is expected that these scaffolds, that revealed to be bioactive, *in vivo* will form a tight chemical bond to the living bone through the apatite layer promoting bone regeneration and better acceptance by the body. The formation of bone-like apatite layer on scaffolds immersed in RPMI 1640 medium is not so apparent (Fig. B2 and B3 in Appendix B) as in SBF, especially when looking to SEM images of G5 after 1 week immersion (Fig. B3 B.1 in Appendix B) because it is known that proteins present in the serum added to the culture medium bind the  $Ca^{2+}$  ions forming calcium proteins in solution, which slows down the precipitation process (66,79).

The *in vitro* biological response of cells when in contact with the scaffolds is a major needed evaluation that will dictate the *in vivo* use. The viability assay accomplished in the present study on osteosarcoma MG-63 cell line showed no toxic effect of the scaffolds with the values of cellular viability close to the control group (G1: PLA-Col) and to each other (Fig. 4.11), which indicates that none of the scaffolds components (nHA, SPIONs and MH) negatively influence the cytocompatibility of the scaffolds. In the first cell viability measurement (Fig. 4.11 Week 2), G5: PLA-Col-nHA-SPIONs-MH presented significant less cellular viability compared to the other groups possible due to the burst release of MH in the first hours that was seen in the MH release assay (Fig. 4.7), nevertheless the cellular viability rapidly recovered over the weeks perhaps because of the knowing capacity of MH to enhance cell adhesion, viability and proliferation (80). Earlier in this study, it was verified that SPIONs, by themselves, are able to induce ROS production (Fig. 4.2), although not in the amount necessary to lead to death of cancer cells, because of that it was expected that scaffolds functionalized with SPIONs also did not present a ROS production capable of provoking cell death. The scaffolds oxidative assay revealed what was expected (Fig. 4.12), being any of the scaffolds group capable to significantly induce the production of the necessary amount of ROS to lead to cancer cell death, which are in concordance with the cellular viability assay, where no cytotoxicity was verified. In overall, the five groups of scaffolds are biocompatible, which will enhance, *in vivo*, the interaction between the implanted material and osteoblasts (76), being promising candidates for the *in vivo* assays.

Osteogenic capacity is one of the main goals of scaffolds to achieve ideal bone tissue regeneration and can be identified by the activity of the enzyme ALP and by the formation of calcium deposits. ALP activity is an earlier indicator of the differentiation into osteogenic lineage and in previous studies Cecen B. et al. showed that PLLA scaffolds with collagen raise the ALP activity on MG-63 cells (59), and knowing that although MG-63 cells are already differentiated into osteoblast and exhibit a low basal ALP activity (81), it is possible to affirm that the ALP activity observed in these scaffolds results from the capacity of them to promote the ALP activity (Fig. 4.13 A.). However, there were no significant difference between the groups of scaffolds, which indicates that ALP increased activity resulted from the combination of PLA and collagen, and not

from none of the remaining components added to the scaffolds. This affirms the osteoconductive properties of PLA and the importance of collagen for bone tissue regeneration (82). Although knowing that hydroxyapatite have osteogenic potential, Zhang X. et al. and Causa F. et al. (73,83) realized that human osteoblasts and Saos-2 cells responds differently to different doses of hydroxyapatite, inducing osteoblastic cell differentiation in a dose dependent manner, which may explain why hydroxyapatite scaffolds do not increase ALP activity, because nHA concentration is not adjusted. On the other hand, scaffolds loaded with nHA showed significantly higher quantity of calcium deposits (Fig. 4.13 B.), which indicates bone mineralization and ECM formation. The calcium deposition by MG-63 cells occurred due to the presence of nHA, an external supply of calcium ( $\text{Ca}^{2+}$ ), that has already been showed to influence the matrix mineralization by Takagishi Y. et al., where the authors concluded that the mineralization of MG-63 cells is accelerated when a source of high content in  $\text{Ca}^{2+}$  is supplied (17). The formation of mineralized matrix is a phenotype marker for a later stage of osteogenic differentiation which is anticipated by the down-regulation of ALP activity, being a signal for the initiation of the mineralization phase (17,73). This suggests that MG-63 cells on the date of the ALP activity and Alizarin Red assays were in a late differentiation stage of osteoblasts, where MG-63 cells recognize the high content of  $\text{Ca}^{2+}$  that cause the enhancement of mineralization but without varying other differentiation markers, in this case without changing the ALP activity marker (17). In overall, nHA enhance osteogenic capacity of scaffolds by inducing bone mineralization and the PLA-Col also promote osteogenic capacity making the scaffolds promising candidates for bone regeneration applications.

In hyperthermia studies, SPIONs by themselves showed a slowly raise in temperature (Fig. 4.14 A.) of the solution from 35.5°C to 42.5°C after 30 mins, however it is not enough to achieve the clinically meaningful temperature increase, that is the raise by 3 - 5°C in the first five minutes of exposure to the AMF (20), not reaching the temperatures needed to destroy the remaining cancer cells in a clinically feasible time. This is possible due to the low SPIONs concentration, by increasing it, in a range where it is not cytotoxic for cells, could be a promising hypothesis to achieve the hyperthermia results desire to apply clinically. PLA scaffolds revealed no increasing of temperature resulting from the presence of SPIONs, this is because the concentration adsorbed at PLA surface is even less than 1 mg/mL. So, it is needed to choose a higher SPIONs concentration and a better method to control and achieve the desire concentration in the PLA scaffold, for example by printing the polymer already with the nanoparticles incorporated (9). Also, it is needed to have a closer look at the experimental methodology, including the equipment, the surrounding environment, how the temperature is measured and the parameters (frequency and amperage) used, that might not be the most appropriate to evaluate hyperthermia with a clinical purpose and search for better ones that closely resembles what occurs in the human body.



# 6.

## 6 Conclusions

The present study sought to develop an effective alternative to the actual bone cancer treatment that faces a variety of limitations and fails in terms of promoting bone regeneration with the use of auto- and allografts and in preventing tumour recurrence by using the recurrent methods of chemo- and/or radiotherapy. A search for adequate characteristics, biomaterials and techniques to achieve the goals listed before led to the fabrication of 3D-printed PLA scaffolds by FDM technique, that physically supports bone regeneration, functionalized with different elements that allows to achieve multiple purposes at once: collagen and hydroxyapatite nanoparticles to enhance bone cells regeneration and mineralization (osteogenic potential), iron oxide nanoparticles to be able to apply magnetic heating hyperthermia as alternative to chemo- and radiotherapy, and antibiotic minocycline to prevent surgery and implant associated infection. The novelty of these scaffolds is the dual-delivery of treatment molecules, SPIONs and MH, on the precise target once they are incorporated in scaffolds surface. Associated with compounds responsible for osteogenic promotion (nHA), results in a versatile scaffold with the combination of antimicrobial/antibiofilm properties, osteogenic properties and with magnetic heating properties.

PLA scaffolds with controlled architecture and macroporosity were successfully obtained by 3D-printing technique and their surfaces were successfully functionalized with the molecules mentioned before, observed by SEM imaging and confirmed by EDS analysis. Looking at the scaffolds group that gather all the compounds (G5: PLA-Col-nHA-SPIONs-MH), it was demonstrated a swelling ability proper for bone regeneration allowing the presence of liquid without losing or deforming the initial structure. The two-phase minocycline release profile revealed to be adequate for therapeutic applications being higher enough to have antimicrobial/antibiofilm effect against *S. aureus*, a major pathogen in associated bone infection, without being cytotoxic to MG-63 cells. In SBF immersion, scaffolds from G5 exhibited the formation of a shiny apatitic layer that indicates good bioactivity, which is important to enhance the interface between the material and the bone tissue and important for cell proliferation. Functionalized PLA scaffolds demonstrated no cytotoxic effect on MG-63 cells being cells actively proliferating on the surface. nHA improved osteogenic capacity of scaffolds by promoting the mineralization process visible by the increased quantity of calcium deposits, ALP activity did not suffer variation possible due to the high level of MG-63 cells maturation. The SPIONs presence made ROS production expected, what was not seen possibly due to the low SPIONs concentration. The magnetic heating properties of SPIONs exists but were not enough to reach

hyperthermia temperatures (40-45°C), revealing an even lower ability to raise the temperature when associated with scaffolds, which is probably caused by the low SPIONs concentration that is adsorbed at scaffolds surface and it's a process that cannot be controlled. This issue could be addressed by trying higher magnetic field intensities, increasing SPIONs concentration or by incorporating the SPIONs into the PLA and 3D-printing both together to achieve a controlled SPIONs concentration in scaffolds.

In conclusion, the results of the multifunctionalized PLA 3D-printed scaffolds suggests that they have a considerable potential to be used in treatment and regeneration of bone defects caused by bone tumours through a combination of enhanced osteogenic activity, an adequate therapeutic delivery of antimicrobial dose of antibiotic and with promising magnetic hyperthermia properties, that need to be improved. However, there is room for improvement and more studies to assess the effectiveness of these scaffolds are needed, namely *in vitro* studies on mesenchymal stem cells (MSCs) to investigate the osteogenic capacity of scaffolds to promote cell differentiation into bone cells, genetic assays to quantify the expression of bone related genes on MSCs, *in vitro* magnetic hyperthermia studies to conclude about effectiveness to cause cell death and then, when the variants of scaffolds are all optimized, proceed to *in vivo* studies.



## 7 References

- [1] Tran N, Webster TJ. Nanotechnology for bone materials. *Wiley Interdiscip Rev Nanomedicine Nanobiotechnology*. 2009;1(3):336–51.
- [2] Mohamed AM. An overview of bone cells and their regulating factors of differentiation. *Malaysian J Med Sci*. 2008;15(1):4–12.
- [3] Van Rijt S, Habibovic P. Enhancing regenerative approaches with nanoparticles. *J R Soc Interface*. 2017;14(129):20170093.
- [4] Meng J, Xiao B, Zhang Y, Liu J, Xue H, Lei J, et al. Super-paramagnetic responsive nanofibrous scaffolds under static magnetic field enhance osteogenesis for bone repair in vivo. *Sci Rep*. 2013;3:2655.
- [5] Martin V, Bettencourt A. Bone regeneration: Biomaterials as local delivery systems with improved osteoinductive properties. *Mater Sci Eng C*. 2018;82:363–71.
- [6] Barba A, Maazouz Y, Diez-Escudero A, Rappe K, Espanol M, Montufar EB, et al. Osteogenesis by foamed and 3D-printed nanostructured calcium phosphate scaffolds: Effect of pore architecture. *Acta Biomater*. 2018;79:135–47.
- [7] Kimna C, Deger S, Tamburaci S, Tihminlioglu F. Chitosan/Montmorillonite composite nanospheres for sustained antibiotic delivery at post-implantation bone infection treatment. *Biomed Mater*. 2019;14(4):044101.
- [8] Ma H, Li T, Huan Z, Zhang M, Yang Z, Wang J, et al. 3D printing of high-strength bioscaffolds for the synergistic treatment of bone cancer. *NPG Asia Mater*. 2018;10:31–44.
- [9] Zhang J, Zhao S, Zhu M, Zhu Y, Zhang Y, Liu Z, et al. 3D-printed magnetic Fe<sub>3</sub>O<sub>4</sub>/MBG/PCL composite scaffolds with multifunctionality of bone regeneration, local anticancer drug delivery and hyperthermia. *J Mater Chem B*. 2014;2(43):7583–95.
- [10] Biermann JS, Chow W, Reed DR, Lucas D, Adkins DR, Agulnik M, et al. NCCN Guidelines © Insights Bone Cancer, Version 2.2017. *J Natl Compr Cancer Netw*. 2017;15(2):155–67.
- [11] Valery PC, Laversanne M, Bray F. Bone cancer incidence by morphological subtype: a global assessment. *Cancer Causes Control*. 2015;26(8):1127–39.
- [12] Mantyh PW. Bone Cancer Pain: From Mechanism to Therapy. *Curr Opin Support Palliat Care*. 2014;8(2):83–90.
- [13] Filippidis D, Mavrogenis AF, Mazioti A, Palialexis K, Megaloikononimos PD, Papagelopoulos PJ, et al. Metastatic bone disease from breast cancer: a review of minimally invasive techniques for diagnosis and treatment. *Eur J Orthop Surg Traumatol*. 2017;27(6):729–36.
- [14] Morelli S, Salerno S, Holopainen J, Ritala M, De Bartolo L. Osteogenic and osteoclastogenic differentiation of co-cultured cells in polylactic acid-nanohydroxyapatite fiber scaffolds. *J Biotechnol*. 2015;204:53–62.
- [15] Farzin A, Hassan S, Emadi R, Etesami SA, Ai J. Comparative evaluation of magnetic hyperthermia performance and biocompatibility of magnetite and novel Fe-doped hardystonite nanoparticles for potential bone cancer therapy. *Mater Sci Eng C*. 2019;98:930–8.
- [16] Turnbull G, Clarke J, Picard F, Riches P, Jia L, Han F, et al. 3D bioactive composite scaffolds for bone tissue engineering. *Bioact Mater*. 2018;3(3):278–314.
- [17] Takagishi Y, Kawakami T, Hara Y, Shinkai M, Takezawa T, Nagamune T. Bone-Like Tissue Formation by Three-Dimensional Culture of MG63 Osteosarcoma Cells in Gelatin Hydrogels Using Calcium-Enriched Medium. *Tissue Eng*. 2006;12(4):927–37.

- [18] Danoux CB, Barbieri D, Yuan H, Bruijn JD de, Blitterswijk CA van, Habibovic P. In vitro and in vivo bioactivity assessment of a polylactic acid/hydroxyapatite composite for bone regeneration. *Biomater*. 2014;4:e27664.
- [19] Tayton E, Purcell M, Aarvold A, Smith JO, Briscoe A, Kanczler JM, et al. A comparison of polymer and polymer-hydroxyapatite composite tissue engineered scaffolds for use in bone regeneration. An in vitro and in vivo study. *J Biomed Mater Res - Part A*. 2014;102(8):2613–24.
- [20] Wu VM, Huynh E, Tang S, Uskoković V. Brain and bone cancer targeting by a ferrofluid composed of superparamagnetic iron-oxide/silica/carbon nanoparticles (earthicles). *Acta Biomater*. 2019;88:422–47.
- [21] Ozaki T. Diagnosis and treatment of Ewing sarcoma of the bone : a review article. *J Orthop Sci*. 2015;20(2):250–63.
- [22] Wang X, Li T, Ma H, Zhai D, Jiang C, Chang J, et al. A 3D-printed scaffold with MoS<sub>2</sub> nanosheets for tumor therapy and tissue regeneration. *NPG Asia Mater*. 2017;9:e376.
- [23] Polo-Corrales L, Latorre-Esteves M, Ramirez-Vick JE. Scaffold Design for Bone Regeneration. *J Nanosci Nanotechnol*. 2014;14(1):15–56.
- [24] Hildebrandt B, Wust P, Ahlers O, Dieing A, Sreenivasa G, Kerner T, et al. The cellular and molecular basis of hyperthermia. *Crit Rev Oncol Hematol*. 2002;43(1):33–56.
- [25] Martin V, Ribeiro IA, Alves MM, Gonçalves L, Claudio RA, Grenho L, et al. Engineering a multifunctional 3D-printed PLA-collagen-minocycline-nanoHydroxyapatite scaffold with combined antimicrobial and osteogenic effects for bone regeneration. *Mater Sci Eng C*. 2019;101:15–26.
- [26] Ma S, Adayi A, Liu Z, Li M, Wu M, Xiao L, et al. Asymmetric collagen/chitosan membrane containing minocycline-loaded chitosan nanoparticles for guided bone regeneration. *Sci Rep*. 2016;6:31822.
- [27] Zahar A, Kocsis G, Citak M, Puskás G, Domahidy M, Hajdú M, et al. Use of antibiotic-impregnated bone grafts in a rabbit osteomyelitis model. *Technol Heal Care*. 2017;25(5):929–38.
- [28] Moreno M, Amaral MH, Lobo JMS, Silva AC. Scaffolds for Bone Regeneration: State of the Art. *Curr Pharm Des*. 2016;22(18):2726–36.
- [29]. Cojocar FD, Balan V, Popa MI, Lobiuc A, Antoniac A, Antoniac IV, et al. Biopolymers – Calcium phosphates composites with inclusions of magnetic nanoparticles for bone tissue engineering. *Int J Biol Macromol*. 2019;125:612–20.
- [30] Tappa K, Jammalamadaka U. Novel biomaterials used in medical 3D printing techniques. *J Funct Biomater*. 2018;9(1):E17.
- [31] Almeida CR, Serra T, Oliveira MI, Planell JA, Barbosa MA, Navarro M. Impact of 3-D printed PLA- and chitosan-based scaffolds on human monocyte/macrophage responses: Unraveling the effect of 3-D structures on inflammation. *Acta Biomater*. 2014;10(2):613–22.
- [32] da Silva D, Kaduri M, Poley M, Adir O, Krinsky N, Shainsky-Roitman J, et al. Biocompatibility, biodegradation and excretion of polylactic acid (PLA) in medical implants and theranostic systems. *Chem Eng J*. 2018;340:9–14.
- [33] Gritsch L, Conoscenti G, La Carrubba V, Noeaid P, Boccaccini AR. Polylactide-based materials science strategies to improve tissue-material interface without the use of growth factors or other biological molecules. *Mater Sci Eng C*. 2019;94:1083–101.
- [34] Elamparithi D, Moorthy V. On Various Porous Scaffold Fabrication Methods. *Mapana J Sci*. 2017;16(4):47–52.
- [35] Tamay DG, Dursun Usal T, Alagoz AS, Yucel D, Hasirci N, Hasirci V. 3D and 4D Printing of Polymers for Tissue Engineering Applications. *Front Bioeng Biotechnol*. 2019;7:164.
- [36] Ritz U, Gerke R, Götz H, Stein S, Rommens PM. A new bone substitute developed from 3D-prints of polylactide (PLA) loaded with collagen i: An in vitro study. *Int J Mol Sci*. 2017;18(12):E2569.
- [37] Izadi A, Meshkini A, Entezari MH. Mesoporous superparamagnetic hydroxyapatite nanocomposite: A multifunctional platform for synergistic targeted chemo-magnetotherapy. *Mater Sci Eng C*. 2019;101:27–41.
- [38] Sneha M, Sundaram NM. Preparation and characterization of an iron oxide-hydroxyapatite nanocomposite for potential bone cancer therapy. *Int J Nanomedicine*. 2015;10:99–106.

- [39] Wust P, Hildebrandt B, Sreenivasa G, Rau B, Gellermann J, Riess H, et al. Hyperthermia in combined treatment of cancer. *Lancet Oncol.* 2002;3(8):487–97.
- [40] Herea D-D, Danceanu C, Radu E, Labusca L, Lupu N, Chiriac H. Comparative effects of magnetic and water-based hyperthermia treatments on human osteosarcoma cells. *Int J Nanomedicine.* 2018;13:5743–51.
- [41] Dulińska-Litewka J, Łazarczyk A, Hałubiec P, Szafranski O, Karnas K, Karewicz A. Superparamagnetic iron oxide nanoparticles-current and prospective medical applications. *Materials (Basel).* 2019;12(4):E617.
- [42] Spirou S, Basini M, Lasciari A, Sangregorio C, Innocenti C. Magnetic Hyperthermia and Radiation Therapy: Radiobiological Principles and Current Practice †. *Nanomaterials.* 2018;8(6):401.
- [43] Zeng XB, Hu H, Xie LQ, Lan F, Jiang W, Wu Y, et al. Magnetic responsive hydroxyapatite composite scaffolds construction for bone defect reparation. *Int J Nanomedicine.* 2012;7:3365–78.
- [44] Ittrich H, Peldschus K, Raabe N, Kaul M, Adam G. Superparamagnetic iron oxide nanoparticles in biomedicine: Applications and developments in diagnostics and therapy. *RoFo.* 2013;185(12):1149–66.
- [45] Gupta AK, Naregalkar RR, Vaidya VD, Gupta M. Recent advances on surface engineering of magnetic iron oxide nanoparticles and their biomedical applications. *Nanomedicine.* 2007;2(1):23–39.
- [46] Kahmei RDR, Borah JP. Clustering of MnFe<sub>2</sub>O<sub>4</sub> nanoparticles and the effect of field intensity in the generation of heat for hyperthermia application. *Nanotechnology.* 2019;30(3):035706.
- [47] Shah A, Dobrovolskaia MA. Immunological effects of iron oxide nanoparticles and iron-based complex drug formulations: Therapeutic benefits, toxicity, mechanistic insights, and translational considerations. *Nanomedicine Nanotechnology, Biol Med.* 2018;14(3):977–90.
- [48] Hergt R, Dutz S, Müller R, Zeisberger M. Magnetic particle hyperthermia: nanoparticle magnetism and materials development for cancer therapy. *J Phys Condens Matter.* 2006;18:S2919–34.
- [49] Oka C, Ushimaru K, Horiishi N, Tsuge T, Kitamoto Y. Core-shell composite particles composed of biodegradable polymer particles and magnetic iron oxide nanoparticles for targeted drug delivery. *J Magn Magn Mater.* 2015;381:278–84.
- [50] Chen K-H, Chen B-C, Ho C-Y. Hyperthermia Temperature of Magnetic Fluid with Superparamagnetic Nanoparticles Subjected to an Alternating Magnetic Field. *J Nanosci Nanotechnol.* 2018;18(4):3018–23.
- [51] Huang D-M, Hsiao J-K, Chen Y-C, Chien L-Y, Yao M, Chen Y-K, et al. The promotion of human mesenchymal stem cell proliferation by superparamagnetic iron oxide nanoparticles. *Biomaterials.* 2009;30(22):3645–51.
- [52] Liou G-Y, Storz P. Reactive oxygen species in cancer. *Free Radic Res.* 2010;44(5).
- [53] Wei Y, Zhang X, Song Y, Han B, Hu X, Wang X, et al. Magnetic biodegradable Fe<sub>3</sub>O<sub>4</sub>/CS/PVA nanofibrous membranes for bone regeneration. *Biomed Mater.* 2011;6(5):055008.
- [54] Marycz K, Pazik R, Zawisza K, Wiglusz K, Maredziak M, Sobierajska P, et al. Multifunctional nanocrystalline calcium phosphates loaded with Tetracycline antibiotic combined with human adipose derived mesenchymal stromal stem cells (hASCs). *Mater Sci Eng C.* 2016;69:17–26.
- [55] Silva T, Grenho L, Barros J, Silva JC, Pinto R V., Matos A, et al. A minocycline-releasing PMMA system as a space maintainer for staged bone reconstructions-in vitro antibacterial, cytocompatibility and anti-inflammatory characterization. *Biomed Mater.* 2017;12(3):035009.
- [56] Ismail RA, Sulaiman GM, Abdulrahman SA, Marzoog TR. Antibacterial activity of magnetic iron oxide nanoparticles synthesized by laser ablation in liquid. *Mater Sci Eng C.* 2015;53:286–97.
- [57] Thukkaram M, Sitaram S, Kannaiyan SK, Subbiahdoss G. Antibacterial efficacy of iron-oxide nanoparticles against biofilms on different biomaterial surfaces. *Int J Biomater.* 2014;2014:716080.

- [58] Dinali R, Ebrahiminezhad A, Manley-Harris M, Ghasemi Y, Berenjian A. Iron oxide nanoparticles in modern microbiology and biotechnology. *Crit Rev Microbiol*. 2017;43(4):493–507.
- [59] Cecen B, Kozaci D, Yuksel M, Erdemli D, Bagriyanik A, Havitcioglu H. Biocompatibility of MG-63 cells on collagen, poly-L-lactic acid, hydroxyapatite scaffolds with different parameters. *J Appl Biomater Funct Mater*. 2015;13(1):10–6.
- [60] Torres-Hernández Y, Ortega-Díaz G, Téllez-Jurado L, Castrejón-Jiménez N, Altamirano-Torres A, García-Pérez B, et al. Biological Compatibility of a Polylactic Acid Composite Reinforced with Natural Chitosan Obtained from Shrimp Waste. *Materials (Basel)*. 2018;11(8):E1465.
- [61] Spiridon I, Tanase CE. Design, characterization and preliminary biological evaluation of new lignin-PLA biocomposites. *Int J Biol Macromol*. 2018;114:855–63.
- [62] Rampersad SN. Multiple Applications of Alamar Blue as an Indicator of Metabolic Function and Cellular Health in Cell Viability Bioassays. *Sensors*. 2012;12(9):12347–60.
- [63] Pietkiewicz S, Schmidt JH, Lavrik IN. Quantification of apoptosis and necroptosis at the single cell level by a combination of Imaging Flow Cytometry with classical Annexin V/propidium iodide staining. *J Immunol Methods*. 2015;423:99–103.
- [64] Meng J, Zhang Y, Qi X, Kong H, Wang C, Xu Z, et al. Paramagnetic nanofibrous composite films enhance the osteogenic responses of pre-osteoblast cells. *Nanoscale*. 2010;2(12):2565–9.
- [65] Kokubo T, Takadama H. How useful is SBF in predicting in vivo bone bioactivity? *Biomaterials*. 2006;27(15):2907–15.
- [66] Lee JTY, Leng Y, Chow KL, Ren F, Ge X, Wang K, et al. Cell culture medium as an alternative to conventional simulated body fluid. *Acta Biomater*. 2011;7(6):2615–22.
- [67] Dan Y, Liu O, Liu Y, Zhang YY, Li S, Feng X bo, et al. Development of Novel Biocomposite Scaffold of Chitosan-Gelatin/Nanohydroxyapatite for Potential Bone Tissue Engineering Applications. *Nanoscale Res Lett*. 2016;11:487.
- [68] Zapotocky V, Pospisilova M, Janouchova K, Svadlak D, Batova J, Sogorkova J, et al. Fabrication of biodegradable textile scaffold based on hydrophobized hyaluronic acid. *Int J Biol Macromol*. 2017;95:903–9.
- [69] Guo Z, Yang C, Zhou Z, Chen S, Li F. Characterization of biodegradable poly(lactic acid) porous scaffolds prepared using selective enzymatic degradation for tissue engineering. *RSC Adv*. 2017;7(54):34063–70.
- [70] CLSI. Performance standards for antimicrobial susceptibility testing. 27th ed. CLSI supplement M100. Wayne, PA: Clinical Lab Stand Inst. 2017;
- [71] Yuan Z, Memarzadeh K, Stephen AS, Allaker RP, Brown RA, Huang J. Development of a 3D Collagen Model for the In Vitro Evaluation of Magnetic-assisted Osteogenesis. *Sci Rep*. 2018;8(1):16270.
- [72] Adan A, Kiraz Y, Baran Y. Cell Proliferation and Cytotoxicity Assays. *Curr Pharm Biotechnol*. 2016;17(14):1213–21.
- [73] Zhang X, Chang W, Lee P, Wang Y, Yang M, Li J, et al. Polymer-ceramic spiral structured scaffolds for bone tissue engineering: Effect of hydroxyapatite composition on human fetal osteoblasts. *PLoS One*. 2014;9(1):e85871.
- [74] Wang D, Lin H, Jiang J, Jin Q, Li L, Dong Y, et al. Fabrication of long-acting drug release property of hierarchical porous bioglasses/poly(lactic acid) fibre scaffolds for bone tissue engineering. *IET Nanobiotechnology*. 2015;9(2):58–65.
- [75] Berzina-Cimdina L, Borodajenko N. Research of Calcium Phosphates Using Fourier Transform Infrared Spectroscopy. *Infrared Spectroscopy - Materials Science, Engineering and Technology*. 2012. 124–148.
- [76] Zhao Y, Fan T, Chen J, Su J, Zhi X, Pan P, et al. Magnetic bioinspired micro/nanostructured composite scaffold for bone regeneration. *Colloids Surfaces B Biointerfaces*. 2019;174:70–9.
- [77] Marques CF, Olhero SM, Torres PMC, Abrantes JCC, Fateixa S, Nogueira HIS, et al. Novel sintering-free scaffolds obtained by additive manufacturing for concurrent bone regeneration and drug delivery: Proof of concept. *Mater Sci Eng C*. 2019;94:426–36.
- [78] Pontes C, Alves M, Santos C, Ribeiro MH, Gonçalves L, Bettencourt AF, et al. Can Sphorolipids prevent biofilm formation on silicone catheter tubes? *Int J Pharm*.

- 2016;513(1–2):697–708.
- [79] Tas AC. The use of physiological solutions or media in calcium phosphate synthesis and processing. *Acta Biomater.* 2014;10(5):1771–92.
- [80] Lee CK, Shin JI, Cho YS. Protective effect of minocycline against cisplatin-induced ototoxicity. *Clin Exp Otorhinolaryngol.* 2011;4(2):77–82.
- [81] Luo X, Chen J, Song WX, Tang N, Luo J, Deng ZL, et al. Osteogenic BMPs promote tumor growth of human osteosarcomas that harbor differentiation defects. *Lab Investig.* 2008;88(12):1264–77.
- [82] Ferreira AM, Gentile P, Chiono V, Ciardelli G. Collagen for bone tissue regeneration. *Acta Biomater.* 2012;8(9):3191–200.
- [83] Causa F, Netti PA, Ambrosio L, Ciapetti G, Baldini N, Pagani S, et al. Poly- $\epsilon$ -caprolactone/hydroxyapatite composites for bone regeneration: In vitro characterization and human osteoblast response. *J Biomed Mater Res - Part A.* 2006;76(1):151–62.
- [84] Guo C, Xiang M, Dong Y. Surface modification of poly (lactic acid) with an improved alkali-acid hydrolysis method. *Mater Lett.* 2015;140:144–7.
- [85] Arai Y, Sparks DL. ATR-FTIR spectroscopic investigation on phosphate adsorption mechanisms at the ferrihydrite-water interface. *J Colloid Interface Sci.* 2001;241(2):317–26.





# Appendix A

## *In vitro* swelling ability of scaffolds

The five PLA scaffolds groups under evaluation, plus the two additional groups tested for swelling ability revealed a low swelling capacity important for bone regeneration purposes. Also, it is visible that the subjection of PLA scaffolds to the alkali hydrolysis treatment had the expected effect of increasing the hydrophilicity of PLA (Fig. A1 A.), needed for a better biocompatibility and cell attachment (84), being this group the one with a higher swelling percentage at 24 h of the assay, with 24.7%. When adsorbing elements to the scaffolds surface, the swelling capacity decreases (Fig. A1 B.), as expected.

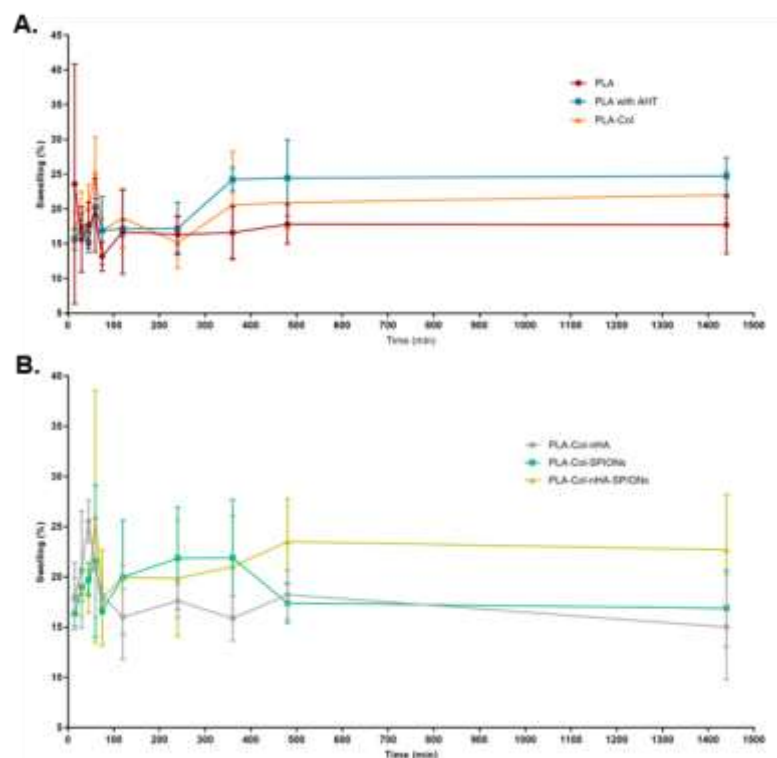
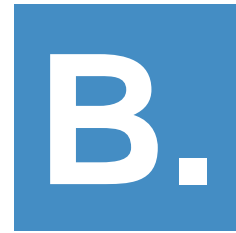


**Figure A1** Swelling ability of PLA scaffolds

Graphic representation of the *in vitro* swelling behaviour of PLA scaffolds (n=3), measured for a period of 24 h (1440 min). In **A.** it is compared the influence of the alkali hydrolysis treatment and in **B.** is observed the swelling ability of the remaining scaffolds groups. It is possible to observe a low swelling ability for all the groups represented here and that the alkali hydrolysis treatment positively influences the PLA scaffolds conferring more hydrophilicity.





## Appendix B

### *In vitro* bioactivity study of scaffolds

Scaffolds from G1: PLA-Col and G3: PLA-Col-SPIONs immersed in SBF solution for different periods of time show no alterations in molecular bond vibration peaks when compared to scaffolds from the same groups that were not subjected to immersion in SBF (Fig. B1 A. and C.), which indicates that apparently in this period of time no bone-like apatite layer was formed on its surface. However, when nHA are adsorbed at scaffolds surface the molecular bond vibration peaks show alterations and deviations in the phosphate and in the -OH group peaks, 1040-1090  $\text{cm}^{-1}$  and 3503  $\text{cm}^{-1}$ , respectively, indicating that probably a bone-like apatite layer has formed at the scaffolds surface. These results allow to say that nHA is the responsible for the promotion of the apatite layer formation and consequent bioactivity (74,75).

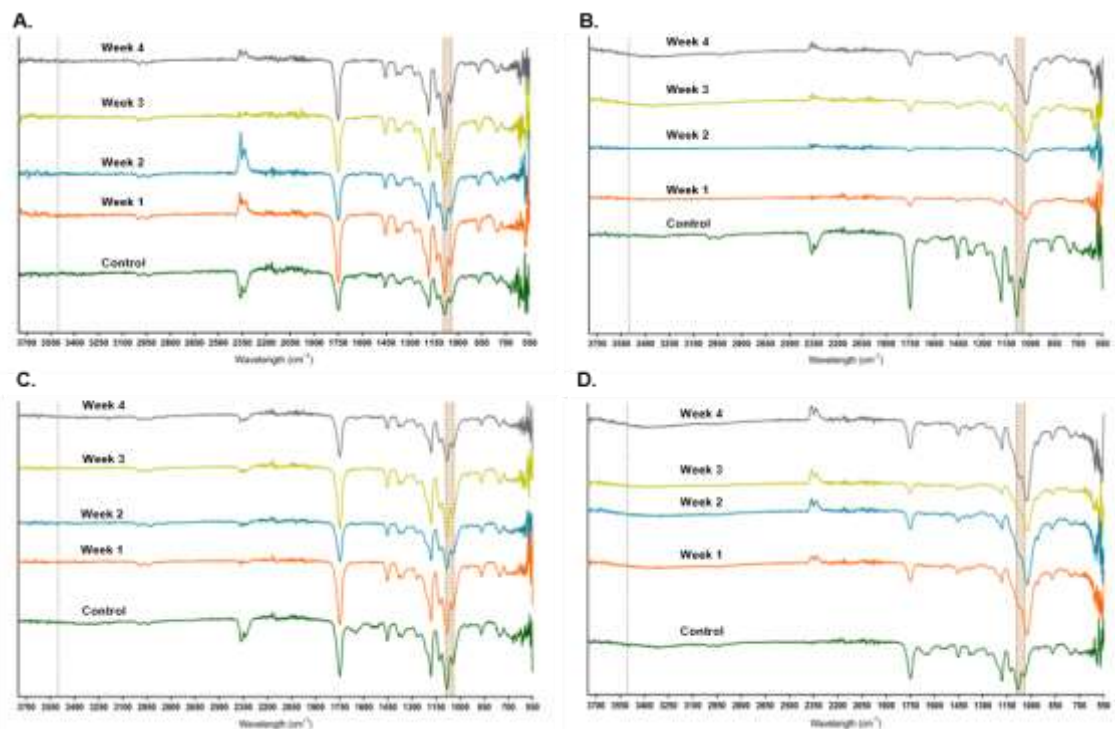


**Figure B1** Bioactivity of PLA scaffolds in SBF solution

Bioactivity evaluation through ATR-FTIR spectra of scaffolds immersed in SBF solution for different periods of time, where **A.** correspond to G1: PLA-Col, **B.** to G2: PLA-Col-nHA, **C.** to G3: PLA-Col-SPIONs and **D.** to G4: PLA-Col-nHA-SPIONs. The scaffolds loaded with nHA present changes in the characteristic peaks of apatite layer that are pointed out at the spectra: 1040-1090  $\text{cm}^{-1}$  to  $\text{PO}_4$  and 3503  $\text{cm}^{-1}$  to -OH group.

Human biological fluids are not only constituted by inorganic ions (e.g.  $\text{Ca}^{2+}$ ,  $\text{Mg}^{2+}$ ,  $\text{Na}^+$ ,  $\text{HPO}_4^{2-}$ ,  $\text{HCO}_3^-$ ,  $\text{K}^+$ ,  $\text{Cl}^-$ ), as is simulated in SBF, they also have amino acids, proteins, sugars, vitamins among other constituents, which causes the use of cell culture medium a closer reality to study the bioactivity of scaffolds (66,79). In the present study, beyond SBF, RPMI 1640 medium was also used to study the bioactivity of scaffolds and the ATR-FTIR spectra are observed in Figure B2 and B3. As observed in SBF, scaffolds from G1: PLA-Col and G3: PLA-Col-SPIONs immersed in RPMI 1640 medium also show no alterations in molecular bond vibration peaks when compared to scaffolds from the same groups that were not subjected to immersion in SBF (Fig. B2 A. and C.). This indicates that, apparently, in this period of time no bone-like apatite layer was formed on its surface, but when nHA are present at scaffolds surface, alterations in the phosphate and in the -OH group peaks ( $1040\text{-}1090\text{ cm}^{-1}$  and  $3503\text{ cm}^{-1}$ , respectively) show alterations, indicating that probably a bone-like apatite layer has formed at the scaffolds surface. The alterations in the apatite characteristic peaks are more pronounced in the G2: PLA-Col-nHA whereof in the G4: PLA-Col-nHA-SPIONs, suggesting less probability of apatite formation in G4, this occurs possible because of the SPIONs presence once it is known that iron oxide ( $\text{Fe}_2\text{O}_3$ ) decreases the ability to form apatite because it bonds with phosphate ions. When comparing G4 in RPMI 1640 medium with SBF solution, the differences are even bigger because, adding to the fact that iron oxide bonds P ions, joins the fact that serum proteins present in the culture medium slow down the precipitation process (65,66,79,85).

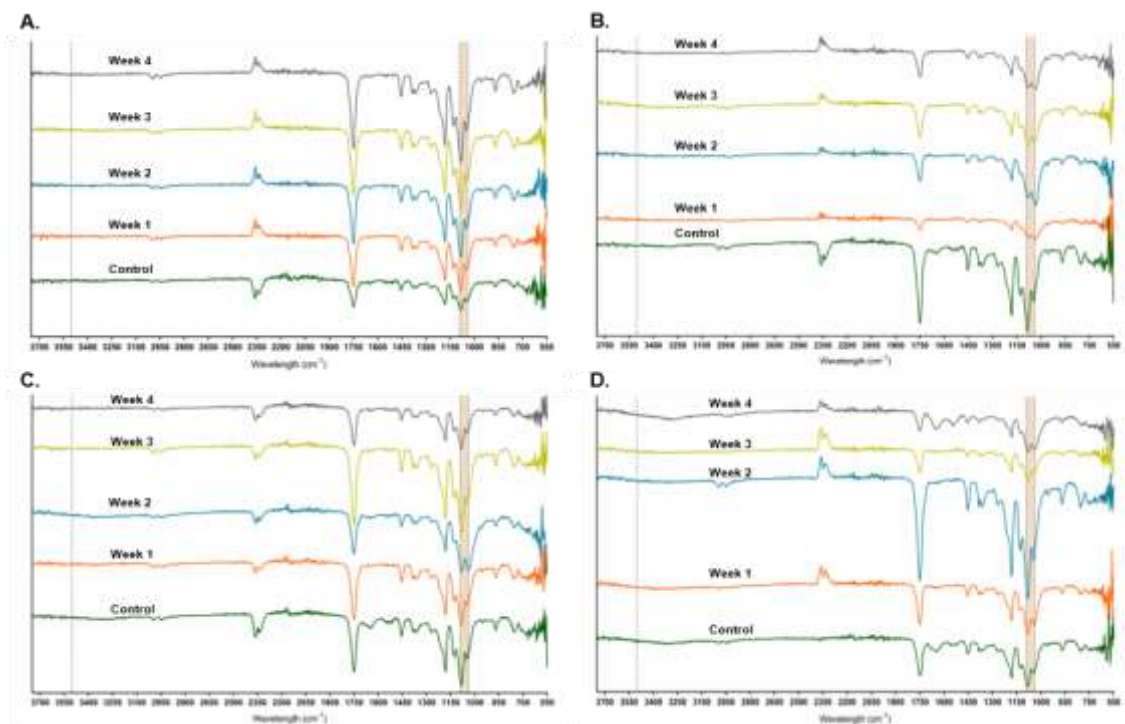


**Figure B2** Bioactivity of PLA scaffolds in RPMI 1640 medium

Bioactivity evaluation through ATR-FTIR spectra of scaffolds immersed in RPMI 1640 medium for different periods of time, where **A.** correspond to G1: PLA-Col, **B.** to G2: PLA-Col-nHA, **C.** to G3: PLA-Col-SPIONs and **D.** to G4: PLA-Col-nHA-SPIONs. The scaffolds loaded with nHA present changes in the characteristic peaks of apatite layer that are pointed out at the spectra:  $1040\text{-}1090$  to  $\text{PO}_4$  and  $3503$  to -OH group.

The G5: PLA-Col-nHA-SPIONs-MH showed alterations and deviations of the phosphate and -OH group peaks (Fig. B3 A.), but the SEM image after the first week immersion on RPMI 1640 medium only shows minimum perturbances of bone-like apatite (Fig. B3 B.1). This difference in the formation of bone-like apatite between RPMI 1640 medium and SBF solution, where a much more evident layer of apatite is formed in SBF solution, is possible due to the fact that the proteins present in the culture medium bind  $\text{Ca}^{2+}$  ions forming calcium proteins in solution, which slows down the precipitation process once the Ca ions are sequestered (66,79).

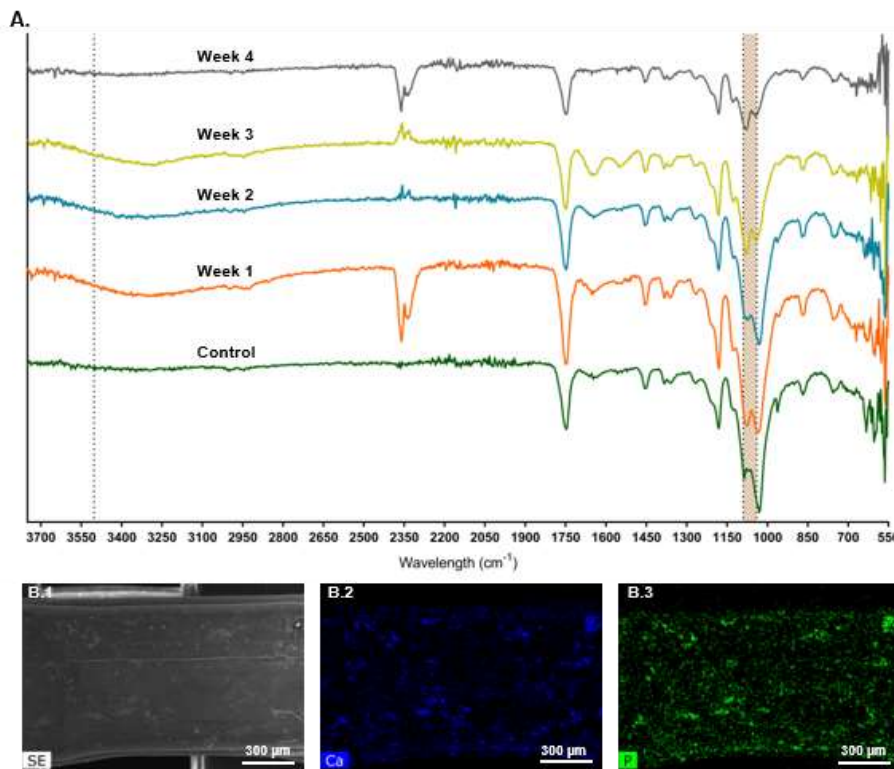


**Figure B3** Bioactivity of G5: PLA-Col-nHA-SPIONs-MH in RPMI 1640 medium ATR-FTIR spectra of scaffolds from G5: PLA-Col-nHA-SPIONs-MH (A.) immersed in RPMI 1640 medium, for different periods of time, to evaluate bioactivity and correspondent SEM image (B.1) and EDS maps of Ca ions (B.2) and P ions (B.3). The ATR-FTIR spectra shows alterations in the characteristic picks of apatite layer that are pointed out at the spectra: 1040-1090 to  $\text{PO}_4$  and 3503 to -OH group. The SEM images and EDS maps show some perturbances formed by Ca and P.

With the formation of a bone-like apatite layer it is known that the pH of the immersion solutions increases by the diminishing of  $\text{H}^+$  that forms -OH groups at the scaffolds' surface, which is verified at the current bioactivity study (Fig. B4), where the pH of the SBF solution increases from 7.4 to approximately 7.8 (Fig. B4 - Grey) in the first week for all scaffolds' group and it is maintained at around 7.8 in the remain weeks. RPMI1640 medium increases from 7.6 to approximately 8.6 (Fig. B4 – Blue) in the first week with a slight increase over the weeks. The more pronounced increase in the pH of the culture medium can be justified by the fact that RPMI 1640 medium needs controlled levels of  $\text{CO}_2$  to maintain the buffering capacity, what was not provided (66).

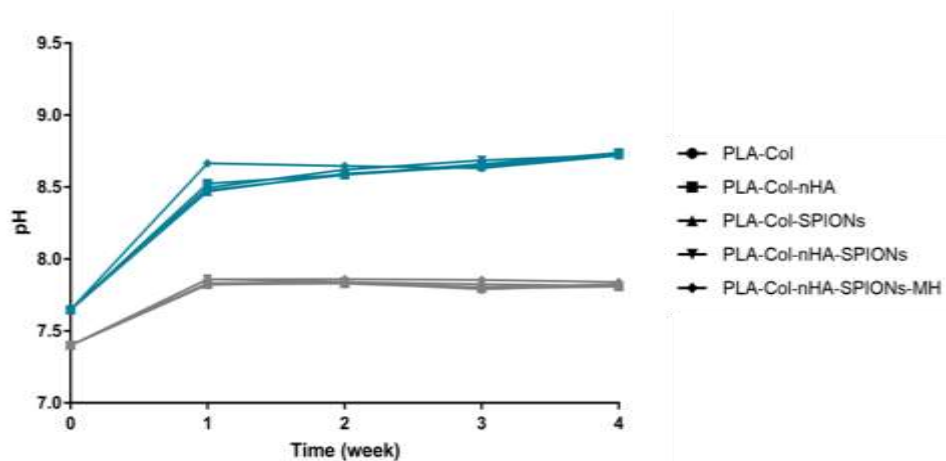
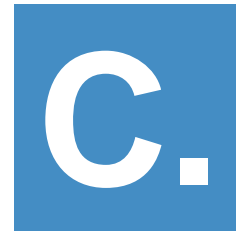


**Figure B4** pH changes of SBF solution and RPMI 1640 medium

Graphic representation of the alteration in the pH solutions after different periods of scaffolds immersion. Grey correspond to SBF solution and blue to the RPMI 1640 medium.



# Appendix C

Poster presented at 4<sup>th</sup> meeting of Colégio de Química da Universidade de Lisboa, Chemistry: Shaping the Future (2019) and at 11<sup>th</sup> iMed.Ulisboa Postgraduate & 4<sup>th</sup> i3DU Students Meeting (2019)

**Polymeric 3D-scaffolds as platforms for local-delivery to the bone**

Ana Sofia Barreira<sup>1,2</sup>, Isabel Florêncio<sup>1</sup>, Ricardo A. Claudio<sup>1</sup>, Maria M. Alves<sup>1</sup>, Maria João Correia<sup>1,2</sup>, Catarina Barreira<sup>1,2</sup>, Lídia M. Gonçalves<sup>1</sup>, Ana F. Bettencourt<sup>1</sup>

<sup>1</sup>Departamento de Ciências da Vida, Faculdade de Ciências e Tecnologia, Universidade Nova de Lisboa, Portugal; <sup>2</sup>Instituto de Investigação em Medicina Molecular (i3M), Faculdade de Medicina, Universidade de Lisboa, Av. Prof. Gama Pires, 1649-003 Lisboa, Portugal; <sup>3</sup>IST Technical University of Lisbon, Campus PIS, 2019 Sacelma, Portugal; <sup>4</sup>CCO, Instituto Superior Técnico, Universidade de Lisboa, Av. Rovisco Pais 1, 1049-001, Lisboa, Portugal

[asbarreira@fcct.unl.pt](mailto:asbarreira@fcct.unl.pt)

### Introduction

Secondary bone cancer is a frequently pathology with a golden standard treatment (surgical resection, radio- or chemotherapy), followed by systemic anti- or radiotherapy [1], which has a variety of limitations and restrictions that need to be replaced by more effective strategies. Sponged polymeric acid (PLA) scaffolds are biocompatible, biodegradable and accomplish several biological and physical requirements for bone regeneration [1] with the additional possibility of design the macro- and microstructures of scaffolds according to the patient's needs. The combination of hydroxyapatite nanoparticles (HA) enhance the osteogenic potential of PLA [2], promote new bone formation, and the combination of metallic nanoparticles (AuNP) allows the administration of the normal cancer cells, to alternatively to classic anti- or radiotherapy, through their specific properties when applied an alternating magnetic field, causing a hyperthermia effect with a local increase of temperature to 43-45°C [3]. Also, the addition of the antibiotic erythromycin (Ery) to PLA decreases the likelihood of an infection and bone a gradual effect on bone regeneration [2]. The aim of this work was to characterize and study the *in vitro* antimicrobial, biocompatibility and osteogenic properties of PLA scaffolds, produced by a 3D-printing technique previously optimized in our group [2], functionalized with different concentrations of HA, AuNP and Ery.

### Results

#### 1. Scaffold characterization

SEM analysis show the presence of both nanoparticles (AuNP and HA) on the surface of PLA scaffolds.

SEM analysis with porous and spongy and AuNP is spherical form, which permits verify the presence of them in the groups with both nanoparticles addition.

The absorption of AuNP and HA were confirmed by EDX analysis.

Adsorption well achieved and stable.

#### 2. Microbiological studies

The group with antibiotic (PLA-Co-**Au**-**HA**-**Ery**) shows an inhibition zone with an average diameter of 22.67 ± 2.33 mm in the Agar diffusion assay.

SEM images of SEM in inhibition assay showed no bacteria formation in the surface of scaffold with HA.

PLA-Co-**Au**-**HA**-**Ery** groups have antibi-  
cultural and antibiotic properties.

#### 3. In vitro cell studies on MG-63 cell line

No cytotoxic effect of the four groups of PLA scaffolds functionalized with different concentrations of AuNP, HA, and Ery by MTT assay.

The osteogenic activity, measured by the ALP activity, has no significant differences between the four groups.

The Alkaline phosphatase activity shows that HA promotes better osteogenic deposition, characteristic from the matrix mineralization.

HA enhances osteogenic capacity of scaffolds.

### Methods

#### Scaffold preparation and functionalization:

Scaffold 3D printing by fused deposition modeling (FDM) → Alkaline Hydrolysis (1.1 NaOH 0.25M + Ethanol 50%) → Wash with Citric Acid 0.5% and H<sub>2</sub>O → 3D sterilization (ethanol 70%) → 3D stored in a desiccator → Scaffolds functionalization: Adsorption method.

#### 1. Scaffold characterization:

- Scanning Electron Microscopy (SEM)
- Energy-dispersive X-ray spectroscopy (EDX)

#### 2. Microbiological studies against *Staphylococcus aureus* (ATCC25923):

- Bactericidal activity
- Agar diffusion assay

#### 3. In vitro studies on MG-63 cell line:

- Cell viability by AlamarBlue assay
- Osteogenic capacity by Alkaline Phosphatase (ALP) activity and Alkaline Phos. assay

### Conclusions

In conclusion, functionalized PLA scaffolds showed promising results to be applied directly to the bone as a dual strategy: promoting bone formation and preventing bone infection. Further studies are needed to evaluate their potential application in bone tumors management.